INTERPRETATION OF 3D RESISTIVITY/IP SURVEYS
VG ZONE, PLATEAU SOUTH PROPERTY

Yukon, Canada

133° 23' W 63° 17' N

November 21, 2014

Prepared for:
Goldstrike Resources Ltd.

Prepared by:

AURORA GEOSCIENCES

TECHNICAL REPORT
INTERPRETATION 3D RESISTIVITY/CHARGEABILITY SURVEY
VG ZONE, PLATEAU SOUTH PROPERTY, YUKON

Effective Date: November 21, 2014

Prepared for:
Goldstrike Resources Ltd.
#1300-1111 West Georgia Street
Vancouver, BC,V6E 4M3
(604) 681 1820
www.goldstrikeresources.com

Prepared by:
Aurora Geosciences Ltd.
34 Laberge Rd, Whitehorse, YT Y1A 5Y9
(867) 668-7672
www.aurorageosciences.com

Authors
Louis Rosenthal,B.SC, G.I.T.
Dave Hildes, Ph.D, P.Geo.

TABLE OF CONTENTS

LIST OF FIGURES

LIST OF TABLES

1. SUMMARY

During the summer of 2014, Aurora Geosciences conducted 3D resistivity and chargeability surveys, and gathered samples for rock physics measurements in the VG, Ben and SW zones of the Plateau South mining property (Figure 1). The purpose of the surveys was to determine the contrast between the resistivity and chargeability of gold-bearing rocks from the host rock, and to guide further exploration.

This report supplements the field report dated September 3rd, 2014 (Appendix 1). Section 2 describes the rock physics analysis conducted on hand samples and core samples. Section 3 describes the steps taken to model the chargeability, resistivity and total magnetic intensity in the survey area. Section 4 describes the models in relation to each other and compares them to the drillhole and geochemical results. A systematic methodology for exploring the area is developed in this section. Section 5 makes recommendations for further exploration on the property. Section 6 is a summary of the key findings of this report and section 7 describes the products included with this report.

Key geophysical properties of 8 hand samples and 5 drill core samples were measured. The samples are divided into 3 categories: felsic volcanics, fault vein and metasediments. Generally the metasediment samples are more conductive and magnetic than the felsic volcanic samples, and slightly less chargeable. One metasediment sample had very high chargeability.The chargeability decay curves of the samples are closely examined, and avariable, the linear decay ratio, which describes their shape is introduced. The linear decay ratio is the most consistent way of distinguishing between the volcanic and the metasedimentary units. An experimental linear decay ratio voxel is created to explore this discriminating property.

As described in the field report, coincident coarse and detail surveys were conducted at the VG Zone and produced two distinct datasets. The coarse models were calculated with a variety of initial models, and the one that converged to the smoothest solution with the best fit to the data is presented here. The two differently scaled datasets were combined by resampling the coarse models to the detail model cell size and using it as a constraint on the detail inversion. This approach is more successful when modelling the chargeability. Magnetic models were constrained using a refocusing/sharpening technique as well as upper and lower bounds.

The results show that the resistivity structure in the near-surface zone consists of a strong NW-SE lineament defined by alternating bands of conductive and resistive rock. A cross-cutting, secondary structure offsets the NW-SE lineament. Chargeability is generally quite low in this upper zone, however there are areas of moderate chargeability that correlate with elevated geochemistry. Deeper, where there is less detail, the models are dominated by a large conductive and chargeable feature under the east half of the survey area.

The models correlate well with the geology of the drillholes, with the exception of the DH13-09 in the SW zone. The transition from felsic volcanic to metasediment in the VG zone is particularly well predicted by the chargeability and ratio models. The correlation analysis of the geochemistry of the drill holes show that gold and arsenic are related to high resistivity, and low to moderate chargeability and low magnetic susceptibility.

The mineralization is restricted to the felsic volcanic unit, which has a low chargeability and high resistivity. Within this unit, targets are generated using a systematic approach which outlines areas of moderate chargeability, similar to the VG zone. Ten target areas are identified and ranked, and drillholes are provided to test each anomaly (Figure 1).

In addition to drill testing targets, a more comprehensive study of the rock physics is recommended to better calibrate the geophysical surveys. This is best achieved with downhole geophysical logging.

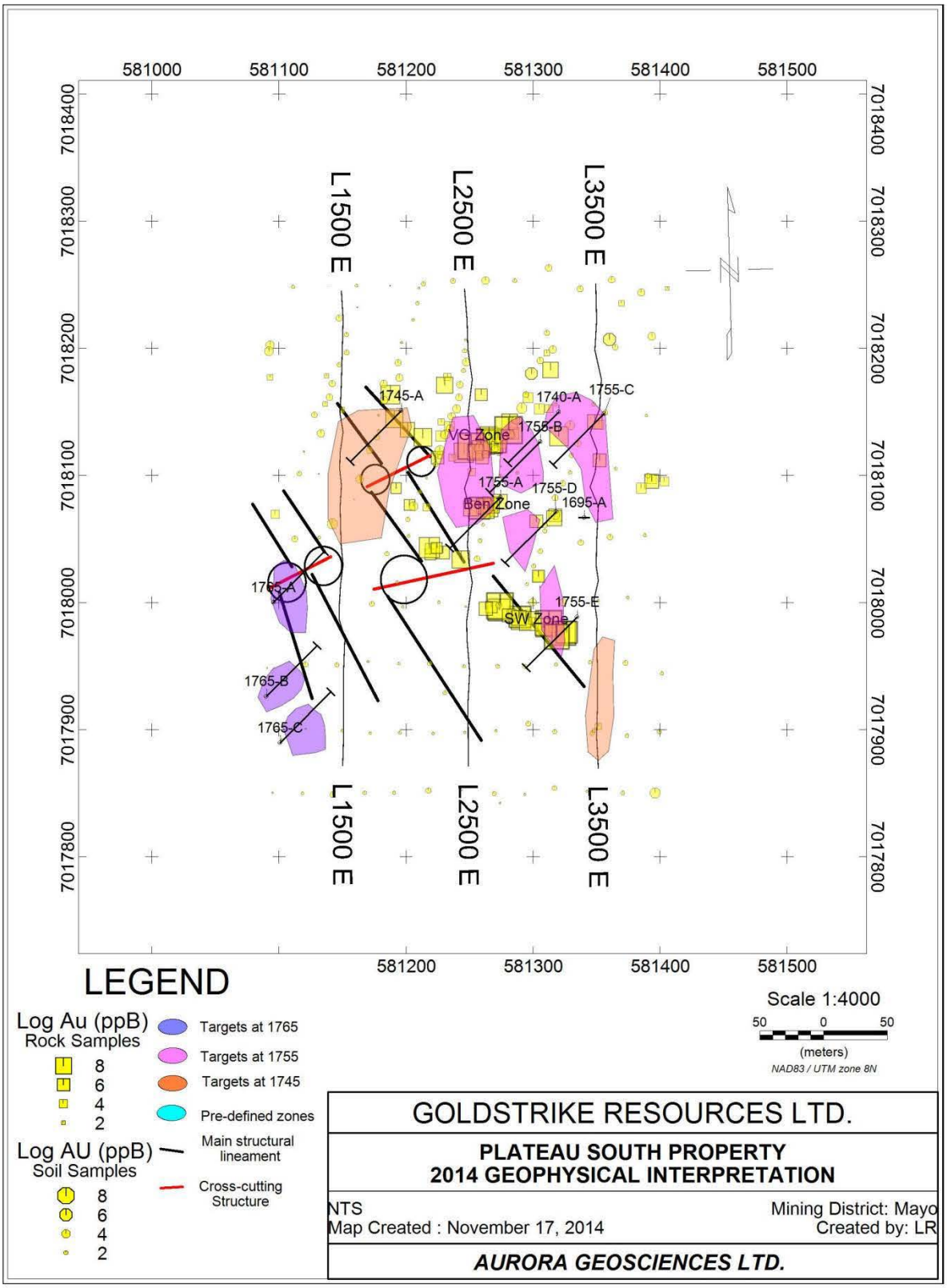

Figure 1: Map showing geochemistry, structural interpretation and the geophysical targets in the survey area.

2. DESCRIPTION OF ROCK PHYSICS RESULTS

A total of 13 representative samples were collected by Daithi Mac Gearailt of Druid Exploration. Aurora personnel measured several physical properties of the samples, including volume, density, resistance, chargeability, magnetic susceptibility and remnant magnetization. Decay analysis was also performed on the chargeability decay curves as an additional tool to differentiate the response of different units. The results are summarized in Table 1, and detailed results are provided in Appendix 2.

The samples are divided in three groups as per the descriptions of Daithi Mac Gearailt: metasediment, felsic volcanic and fault vein. All the samples have low chargeability with the exception of the altered shale samples which displays chargeability an order of magnitude higher than all other samples. On average the felsic volcanic samples are less magnetic, slightly more chargeable and more resistive than the other rocks, although there is significant overlap.

No drillhole samples with high arsenic or gold were included in the rock physics analysis.

Figure 2 shows the decay curves of all samples except the altered shale which is off-scale (high) on this diagram. Generally the felsic volcanic rocks and the fault vein have a higher initial chargeability which mostly decays in the first 200 ms after shutoff. Three of the metasediment samples have a lower initial chargeability which decays more gradually (Figure 3). A new variable, the linear decay ratio, which emphasizes this difference is introduced. The linear decay ratio (Figure 3), defined as the chargeability ratio of the second time gate (80 ms) to the eighth time gate (440 ms). Within the small sample group, excluding a metasediment sample outlier significantly lower than the others, the metasediment samples have a linear decay ratio higher than 2 while the felsic volcanic samples have a linear decay ratio less than 2. There is also a difference in the mean resistivity and mean chargeability between the groups, but linear decay ratio provides a more distinct separation.

A heuristic inversion methodology is proposed to use the ratio for exploration. Datasets of the decay time of IP2 and IP8 were exported, inverted, and a ratio calculated from the recovered models. This model is examined in Section 4.

It is important to note the small amount of samples makes the conclusions in this section tentative. Further rock physics or borehole geophysical logging is recommended to confirm these hypotheses.

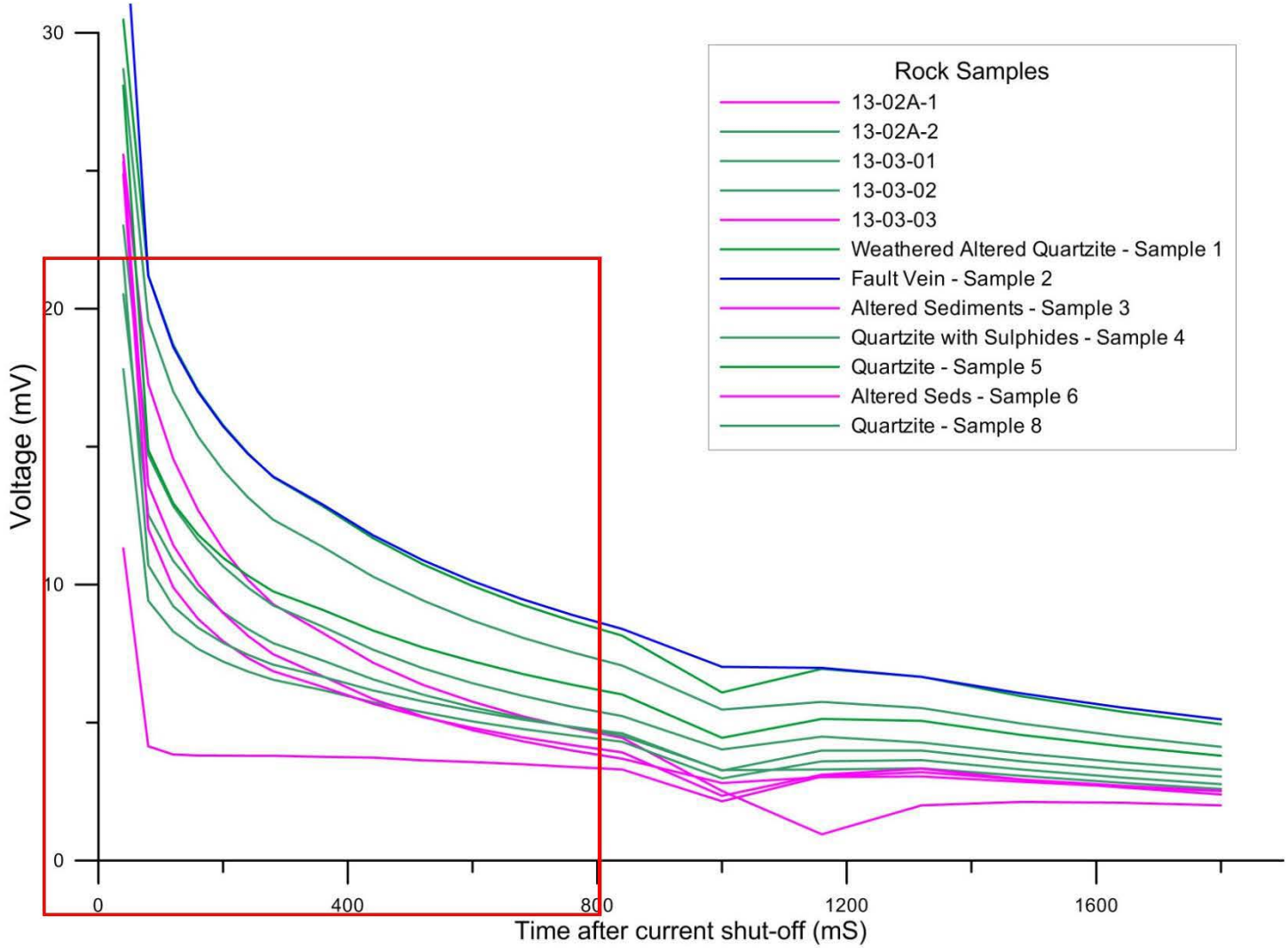

Figure 2: Decay curves of the samples, grouped by color, with green denoting felsic volcanic, blue the fault vein and magenta the metasediments samples. The results from sample 7 is off the scale of this figure. The red rectangle shows the area magnified in Figure 2.

Table 1: Summary of the Rock Physics

Rock Name	Group	Sample type	Resistivity (ohm.m)	Chargeability (mV/V)	Koenigsberger Ratio	Magnetic Susceptibility (x10e3 SI units)	Linear Decay Ratio	Comment
13-02A, 18.2-18.3	Felsic Volcanic	Core sample	7467	6.2	1.09	0.086	1.92	AS PPM: 32.4 AU PPB: 8.5
13-03-1, 21.5-22	Felsic Volcanic	Core sample	931	4.7		0.030	1.91	AS PPM: 55.2 AU PPB: 3.4
13-03-1, 34-34.5	Felsic Volcanic	Core sample	685	5.1		0.018	1.64	AS PPM: 6.9 AU PPB: 0.25
Fault Vein Sample 2	Felsic Volcanic	Grab sample	5208	9.6		0.017	1.80	Typical fault vein material, classic target,
Quartzite - Sample 5	Felsic Volcanic	Grab sample	7498	9.7		0.042	1.81	Typical less altered quartzite
Quartzite - Sample 8	Felsic Volcanic	Grab sample	12641	9.3	0.21	0.021	1.90	Near faults that are potentially mineralized , and show some schistosity,
Quartzite w/ sulphide beds - Sample 4	Felsic Volcanic	Grab sample	3349	5.2		0.038	1.74	Sulphide percentage can vary wildly some dispute as to the possibility of felsic volcanic unitsas seen in the logs
Weathered Altered Quartzite - Sample 1	Felsic Volcanic	Grab sample	3680	6.9		0.028	1.78	Found at the surface near mineralized zone
13-02A-2, 43	Metasediment	Core sample	18382	4.7	0.06	0.118	2.32	AS PPM: 20.1 AU PPB: 3.1
13-03-1, 41-42	Metasediment	Core sample	785	5.2		0.022	2.41	AS PPM: ? AU PPB: ?
Altered mineralized Sediments - Sample 3	Metasediment	Grab sample	1261	3.4		0.213	1.11	Minerals likely Andalucite typically along block faults
Altered Sediments - Sample 6	Metasediment	Grab sample	9742	4.7	0.77	0.067	2.11	Located Close to Mt-Armstrong intrusion, so contact alteration typical of interbeds

Altered Shale, interbedded - Sample 7	Metasediment	Grab sample	1063	93.4	0.029	1.68	Shale beds typical intercepts of various percentages of sulphides, shallow dipping to the south?

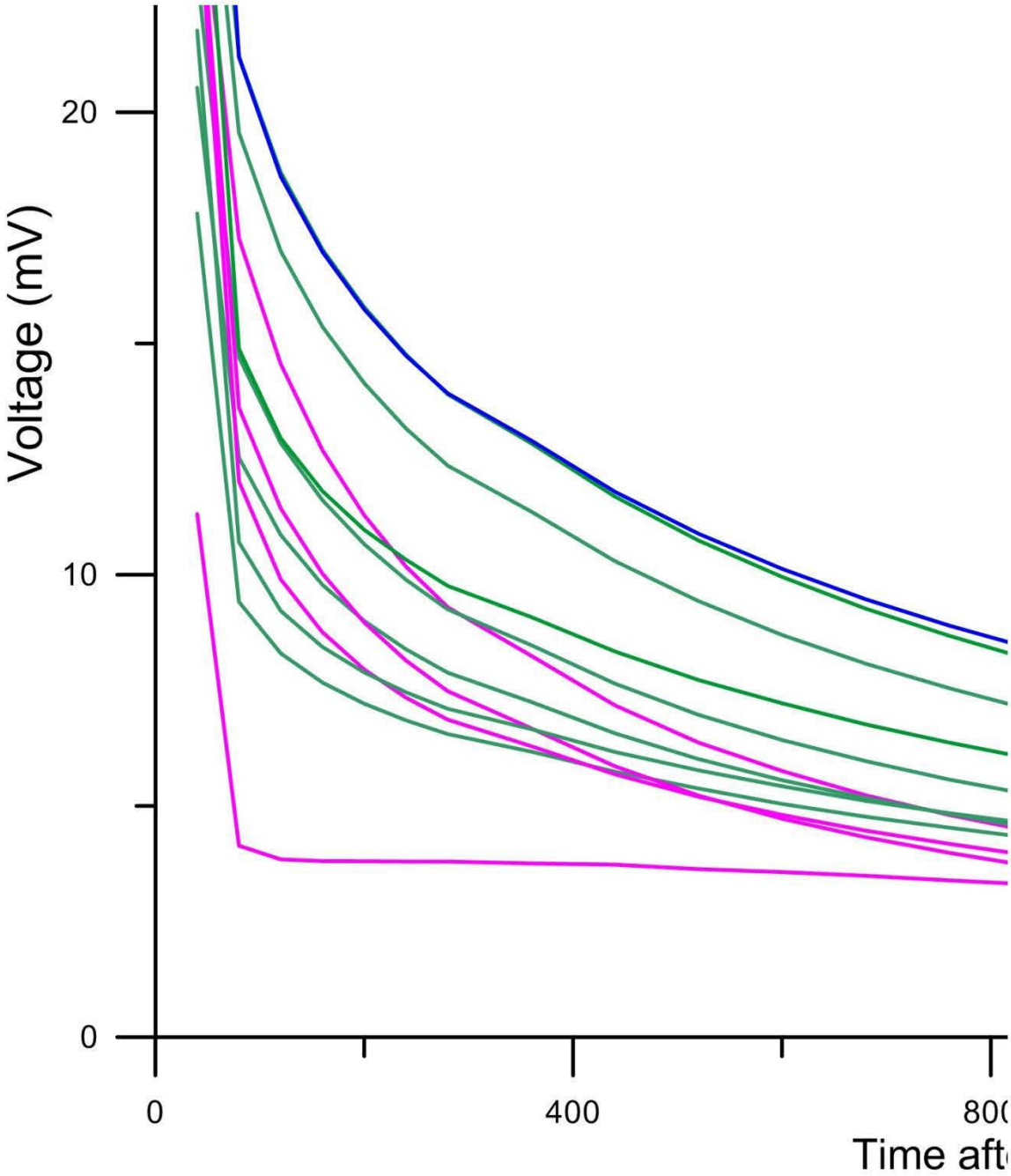

Figure 3: Detailed view of the early time chargeability response of the rock physics. Note how the felsic volcanic samples (green) only intersect the fault vein (blue) and metasediment samples (magenta) but not themselves. This is the basis for the ratio calculation which highlights the difference in slope between the second (80 ms) and ninth (440 ms) time gates.

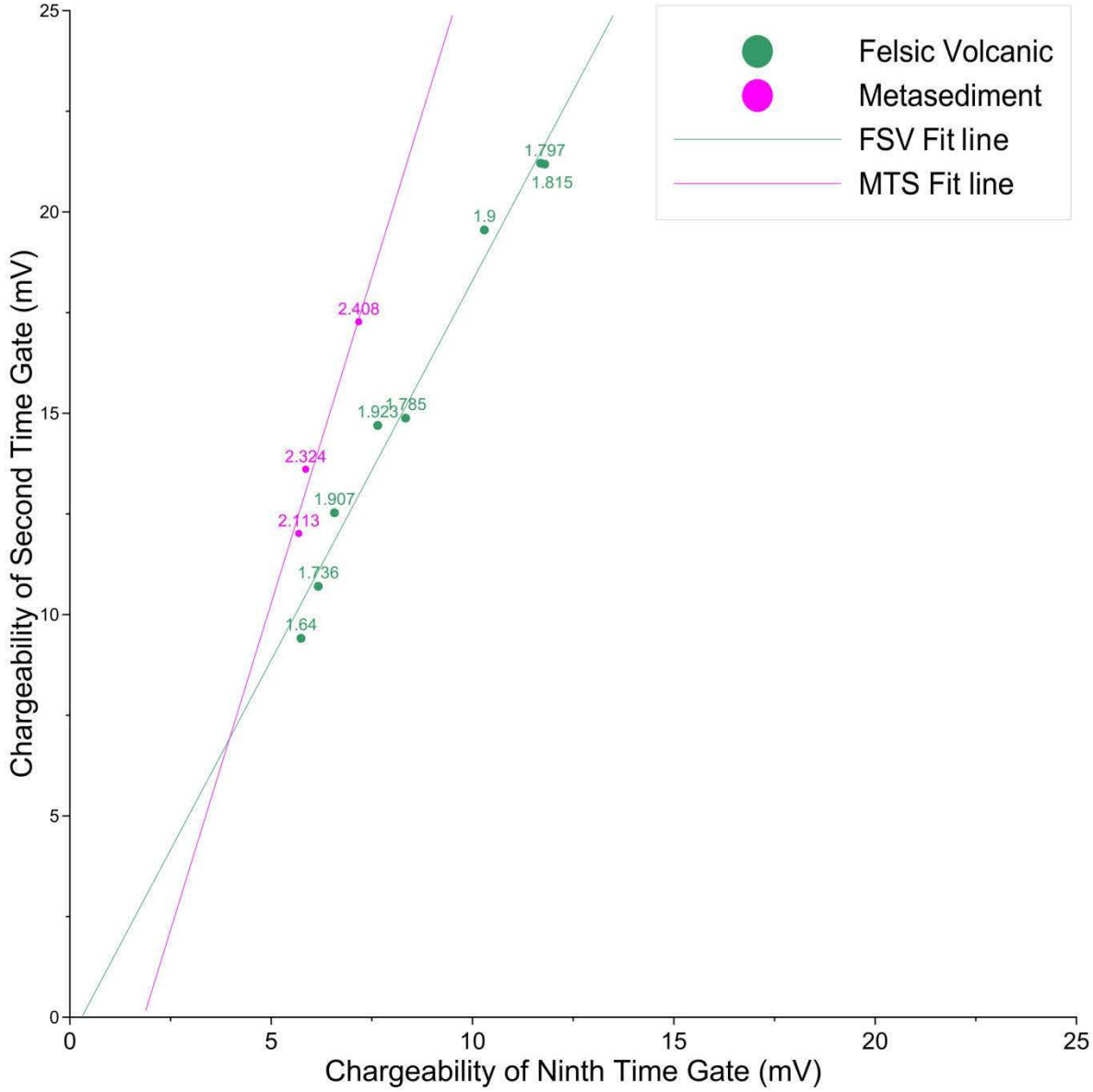

Figure 4: Graphical representation of the linear decay ratio variable, with best fit lines for individual groups. Sample 3 and sample 7 are considered outliers and are not included on this graph.

3. MODELLING

Block earth models of magnetic susceptibility, chargeability and resistivity were created. The RES/IP used the University of British Columbia DCIP3D Inversion code and the susceptibility models were created using Geosoft VOXI. Two separate models were created for each dataset, corresponding to the different resolutions of data. Models are included with this report as UBC models, Geosoft voxels and ASCII (XYZ) format.

3.1 Coarse Recovered Resistivity Model

The coarse resistivity model has a core mesh size of 5 m and a near-surface vertical cell size of 2.5 m. The input data is the *VP_Final* (mV) channel divided by the current (mA). Ten percent of error plus a floor of 0.003 V/A is assigned to each data point prior to inversion. A forward model is calculated from a homogeneous earth with the geometry of each input data to predict the expected polarity of each primary voltage and is applied to the input data. Several generations of quality control were required to create a dataset that converges to a reasonable misfit. The final dataset contains 3420 data from a total of 3690 in the original database. Most data removed had both potential electrodes a similar distance from the current injection point and are therefore very sensitive to uncertainty in the location of the electrodes.

The coarse resistivity model was calculated using a reference and initial model of 2.81187E-04 S/m (3556 ohm.m) and used a weighting file designed to increase the smoothness on the surface. Inversions were also attempted using several different orders of magnitude for initial and reference models to test the sensitivity of the inversion to different assumptions of the average host rock resistivity, most did of these did not converge suggesting that about 3600 ohm-m is the preferred reference value. The inversion converged in 7 iterations and fit the data to a chifact of 1.5, a measure of the goodness of fit demanded from the inversion. The majority of the predicted data points were within 10% of the observed data. Overall, the fit is very good, with all the main features of the observed data being reproduced, and the difference being in the magnitude of some of the more resistive areas. Figures of the predicted, observed and the percent difference between them are included with this report.

3.2 Coarse Recovered Chargeability Model

The coarse chargeability model has the same mesh as the coarse resistivity model. The input data is *IP_final/1000* and *IP_err_final/1000*. A floor of 0.001 V/V was added to the error, to prevent the inversion from over fitting the data. Several generations of quality control were required to create a dataset that would converge to a reasonable misfit. The dataset used to calculate the model included with this report contains 3316 data points from a total of 3690 in the original database. Subsequent to the culling of those data with questionable primary voltages, most of the IP data removed were n=0 or had anomalous decay curves.

Several initial models were tested, and it is determined that an initial model of 30 mV/V lead to the smoothest final model. This moderately high background value is between the high chargeabilities at depth and the lower chargeabilities on surface. The inversion fit the data to a chifact of 1. Overall, the fit is very good, with all the main features of the observed data being reproduced, and the difference being in the magnitude of some of the more chargeable areas. Figures of the predicted, observed and a difference calculation are included with this report.

3.3 Detailed Recovered Resistivity Model

The detailed resistivity model uses a core mesh size of 2.5 m and a vertical cell size of 1.25 m. The input data are the *VP_Final* (mV) divided by the current (mA). Ten percent of error plus a floor of

0.003 V/Aare assigned to the data. A forward model is calculated from a homogeneous earth with the geometry of each input data to predict the expected polarity of each primary voltage and is applied to the input data. Several generations of quality control were required to create a dataset that would converge to a reasonable misfit. The dataset used to calculate the model included with this report contains 3552 data from a total of 4250 in the entire database. All the n=0 and n=1 data were removed prior to the final inversionbecause they created spottiness on surface, caused significant misfit and prevented the inversion from converging.

Models created with different initial and references were attempted, and the best fit to the data used a reference and initial model of 1.94824E-04 S/m (5200 ohm.m) and used 5 layers of top down weighing to reduce spottiness on surface. The inversion converged is 12 iterations and fit the data to a chifact of 1.5. Overall, the fit is very good, with all the main features of the observed data being reproduced. some Figures of the predicted, observed and a difference calculation are included with this report.

3.4 Detailed Recovered Chargeability Model

The detailed chargeability model uses the same mesh as the detailed resistivity model. A floor of 0.001 V/V was added to the error, to prevent the inversion from over fitting the data. Several generations of quality control were required to create a dataset that would converge to a reasonable misfit. The dataset used to calculate the model included with this report contains 3552 data from a total of 4250 in the entire database. The n=0 and n=1 data were removed from the dataset because they created spottiness on surface and caused significant misfit.

The model was calculated using a re-sampled coarse chargeability model onto the detail discretization as the initial and reference model and used 5 layers of top down weighing to reduce spottiness on surface. The inversion converged in 7 iterations and fit the data to a chifact of 0.2. Overall, the fit is very good, with all the main features of the observed data being reproduced. Figures of the predicted, observed and a difference calculation are included with this report.

3.5 Detailed Ratio Model

The ratio model is created by inverting the chargeability from the 80 ms and 440 ms time gates separately, then dividing the 80ms model by the 440 ms model. This is an experimental heuristic tool for differentiating between rock types and highlighting areas of favorable linear decay ratio. The same method was attempted for the coarse models, but at this point in time, a satisfactory results has not been achieved.

3.6 Coarse Magnetic Susceptibility Model

Mesh discretization for the coarse magnetic model is X=12.5, Y=15 and Z= 3m. The sensor height is estimated at 2 m above ground level and the IGRF field is calculated and removed for each data point; the resultant model is an anomalous susceptibility model, not an absolute one. Data were optimized to a single observed datum per cell, and a linear background trend from the dataset was removed prior to inversion. Error of 8% plus a floor of 10 nT is assigned to the data. Constraints consist of upper bound of 0.3, lower bound of -0.3 and an iterative sharpening algorithm was used.

3.7 Detailed Magnetic Susceptibility Model

Mesh discretization for the detail magnetic model is X=2.5, Y=2.5 and Z= 1.25. The sensor height is estimated at 2 m above ground level and the IGRF field is calculated and removed for each data point; the resultant model is an anomalous susceptibility model, not an absolute one. Data were optimized to a single observed datum per cell, and a linear background trend from the dataset was

removed prior to inversion. Error of 8% plus a floor of 10 nT is assigned to the data. Constraints consisted of an upper bound of 0.3 and a lower bound of -0.3 and an iterative sharpening algorithm was used.

4. INTERPRETATION

4.1 Discussion of models

COARSE MODELS

Plan maps of the coarse models are shown in Figure 5, Figure 6 and Figure 7. The resistivity in the survey area is modeled as varying over many orders of magnitude andshows the area to be structurally complex with a dominant NW-SE lineation (black lines in Figure 8) near the surface upset in a few places by a weaker NE-SW lineament (red lines in Figure 8). As shown by the circled areas in Figure 8, the model indicates some evidence of dextral motion along the NE-SW structures; this could produce dilation and consequent focus of fluid flow at these offsets.The recovered resistivity structure has a good correlation with gold values in surface geochemistry, and the VG is in line with one of these cross cutting structures. At depth 1715 and lower, the model is dominated by a large conductive feature that strikes N-S under the southern half of L3500E then veers towards the eastern half of L140N and L180N. This may merely reflect the limit spatial resolution of deep features inherent in the survey technique.

The coarse chargeability model (Figure 6) shows generally low chargeability in the upper 50m, with some areas of embedded, detailed moderate chargeability within the low chargeability layer, particularly on the north-east side of L80N and the center of L140N and L180N. At depths of 1715 and deeper, there is a large thick N-S trending feature under L3500E that veers to the west in the northern part of the survey, close to L140E and L180E. It is largely coincident with the conductivity anomaly mentioned above. This is by far the most chargeable feature in the model, and the only represented unit in the rock physics analysis that could account for this magnitude of chargeability is the altered shale (Table 1, sample 7).

DETAIL MODELS

The detailed resistivity model (Figure 9) showed a similar texture of resistivity, although there is much finer detail here. The response is dominated by a strong conductive feature that intersects L20N obliquely, hitting the center of L80N where it goes north, which is also observed in the coarse data. To the northeast of this is a highly resistive feature which widens considerably under L140N and L180N.

The detailed chargeability model (Figure 10) shows a similar texture to the coarse chargeability model. The NW-SE feature that follows L20N and cuts through the middle of L80N is more prominent and sharp in the detailed model. There are fine moderate chargeability features in the highly resistive complex beneath L140N and L180N.

The detailed magnetic model (Figure 11) shows a corridor of highly variable magnetic susceptibility that roughly correlates to the eastern boundary of the resistive feature that hosts the data. The high variability of the magnetic susceptibility may be in part to irregular remanent magnetism acting in different directions than the Earth's field. The Koenigsberger ratio, an indication of relative strength of remanent to induced magnetization, is greater than one for a single sample in the VG Zone. Some of the dextral motion observed in the coarse resistivity model is also apparent in this model (Figure 8).

The detailed ratio model (Figure 12) has high spatial variability on surface; at 1745 and below it matches well with the lithologies encountered in the drillholes with below 2 (red) indicating felsic volcanic and above 2 (blue) indicating metasediment.

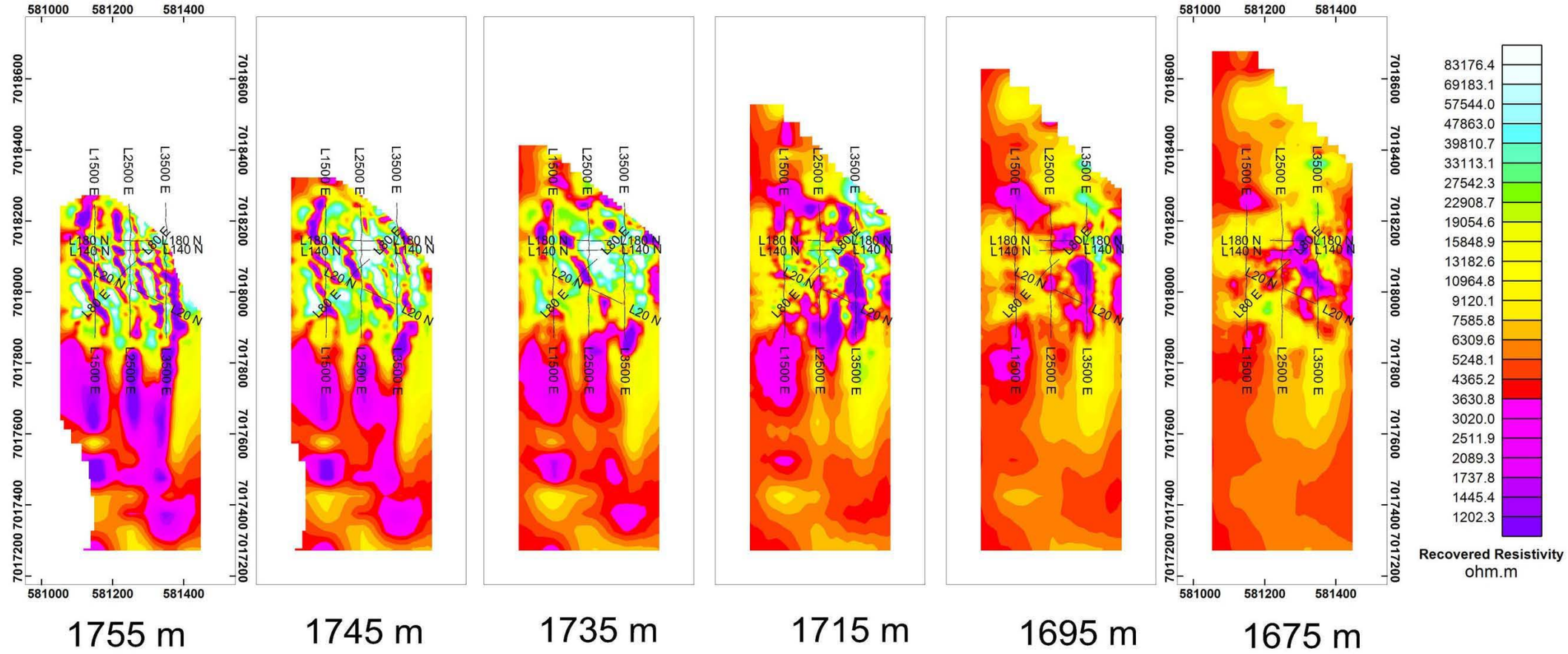

Figure 5: Plan views of the coarse recovered resistivity model at different elevations. North is towards the top of the page.

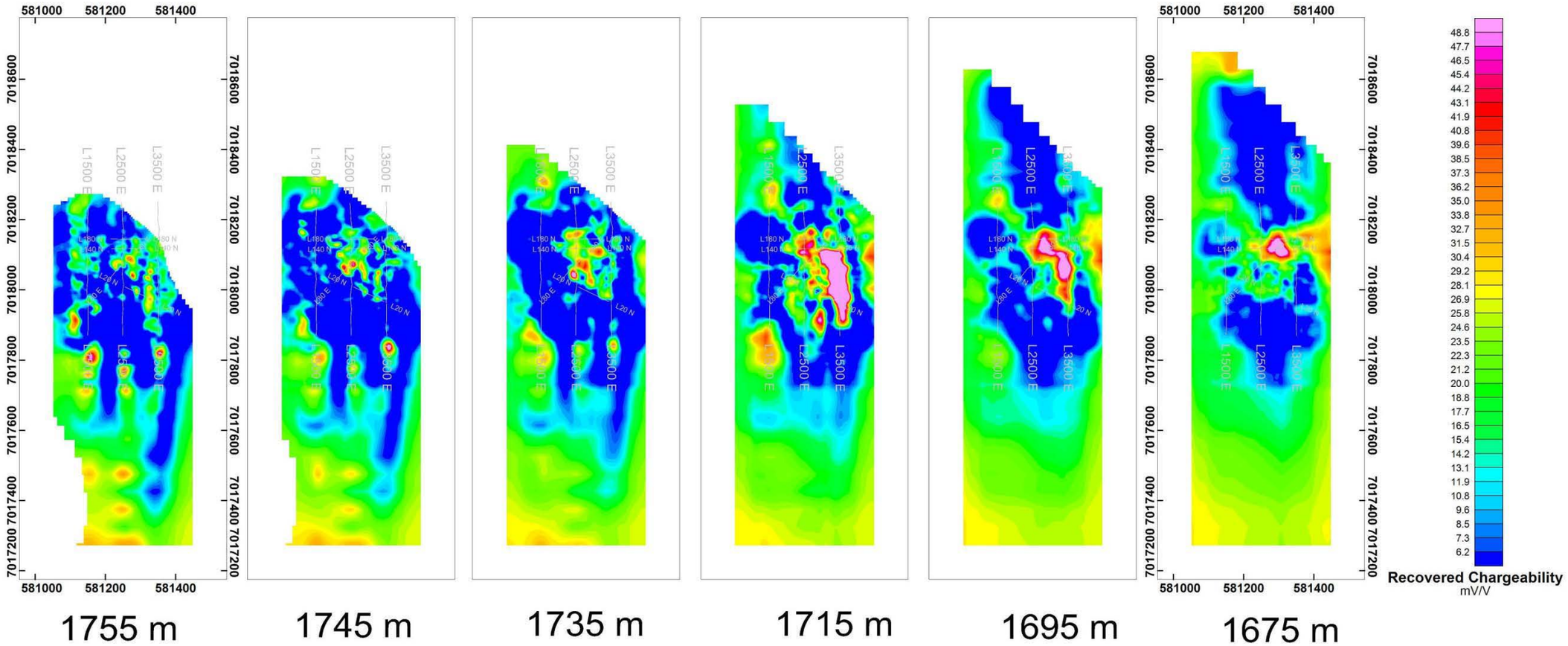

Figure 6: Plan views of the coarse chargeability model at different elevations. North is towards the top of the page.

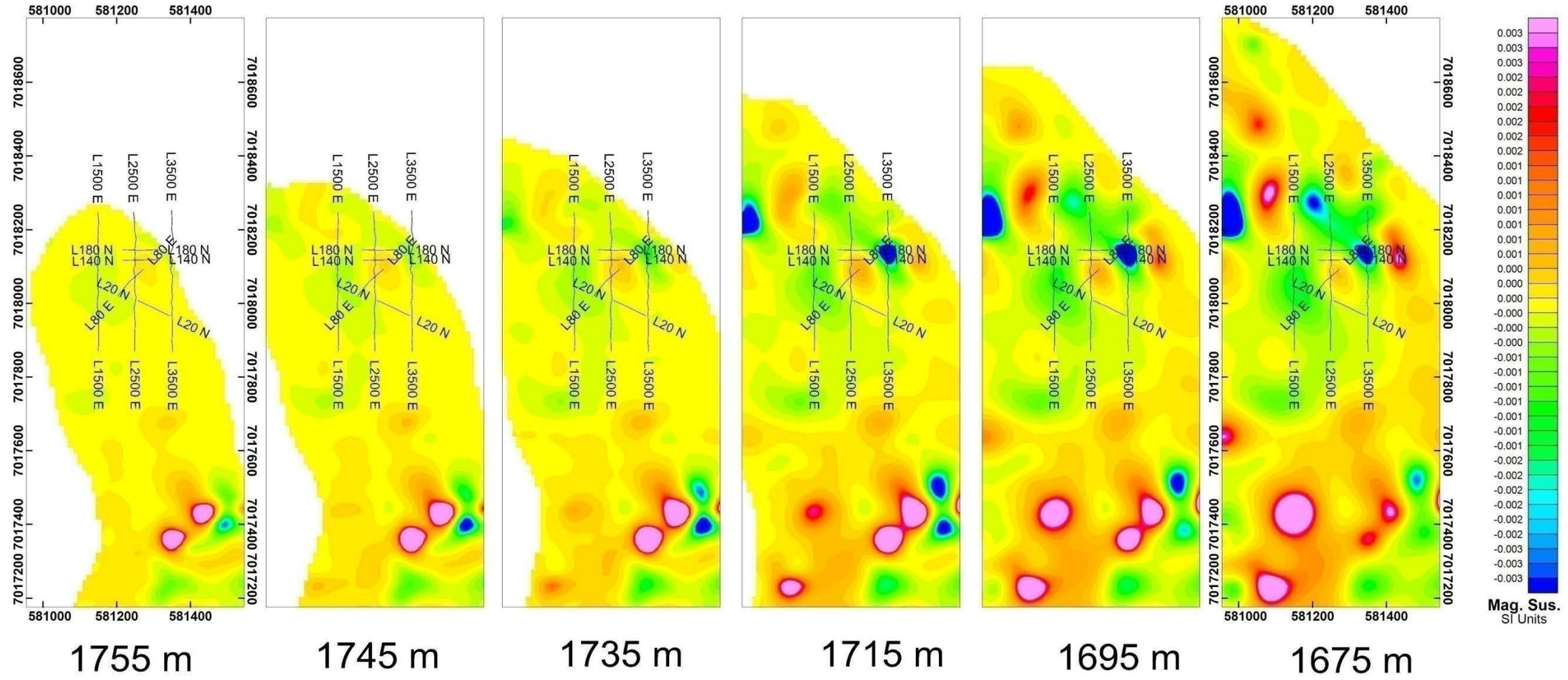

Figure 7: Overview of the magnetic susceptibility model created from the coarse dataset at different elevations.

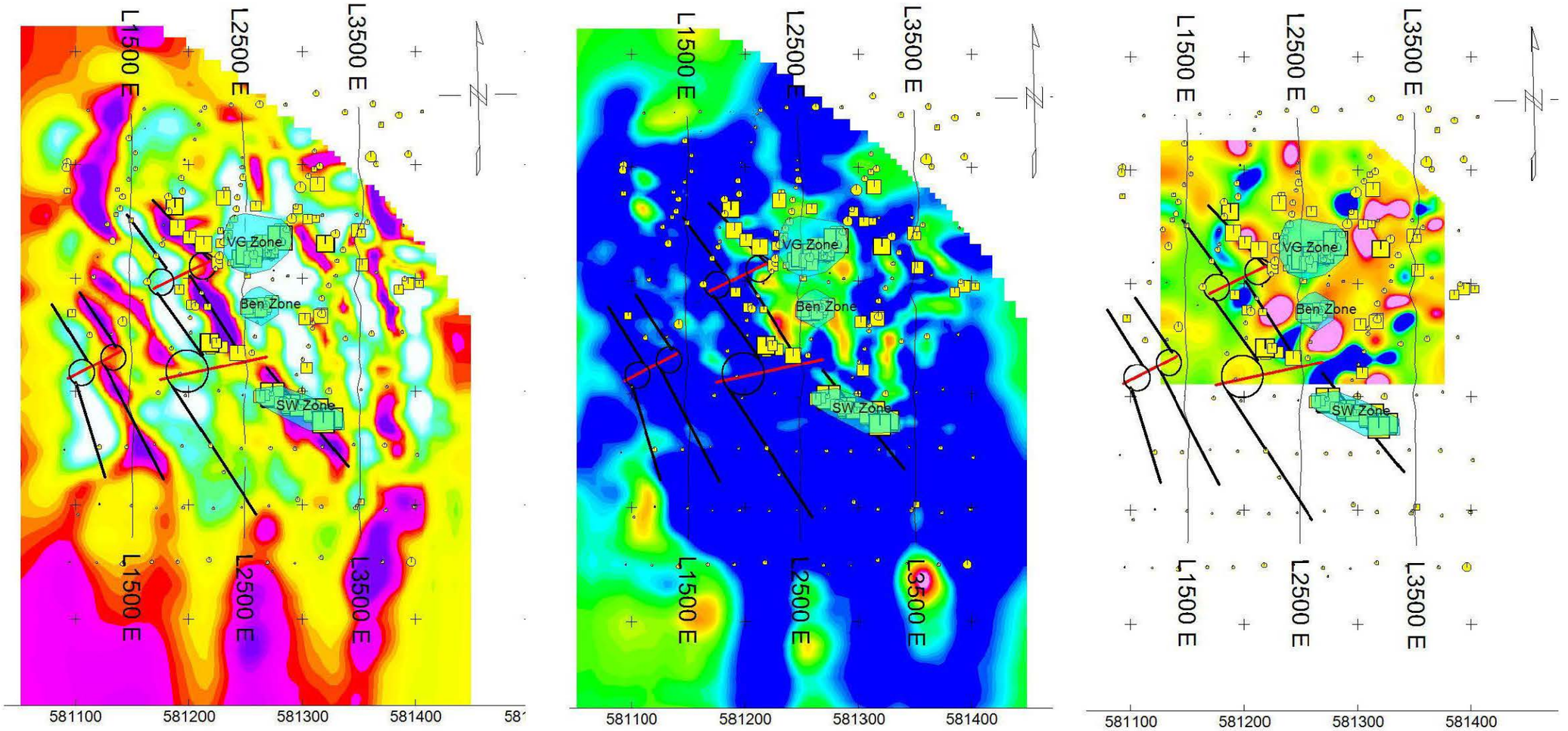

Figure 8: Plan view of the structural interpretation of the area at elevation 1745 with coarse resistivity (left), coarse chargeability (centre) and detail magnetic (right). Black lines indicate the dominant N-S resistivity lineaments and the red lines show the cross-cutting structure. Circles indicate possible dextral movement caused by the cross cutting structures.

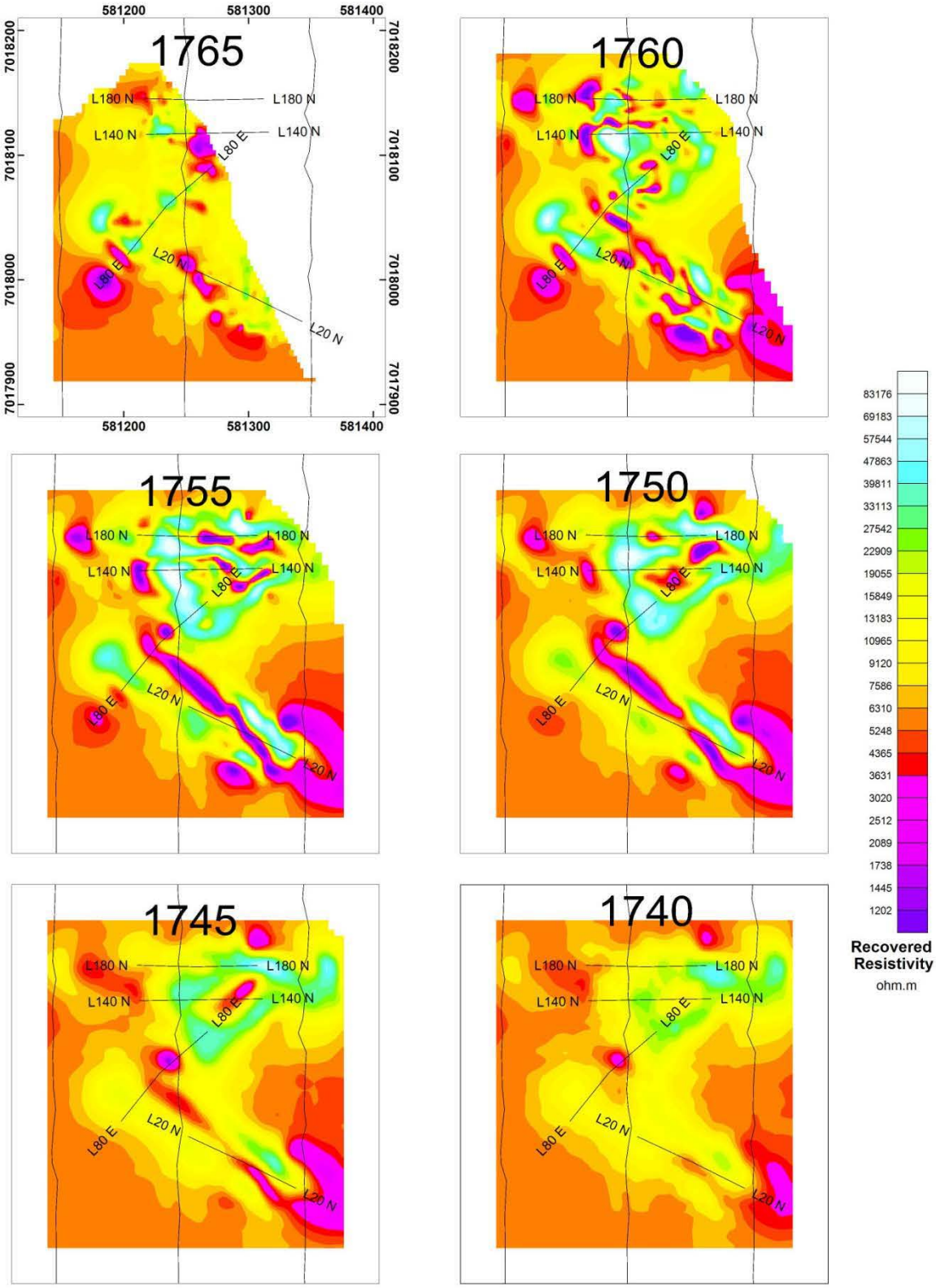

Figure 9: Plan views of the detailed resistivity models. North is towards the top of the page.

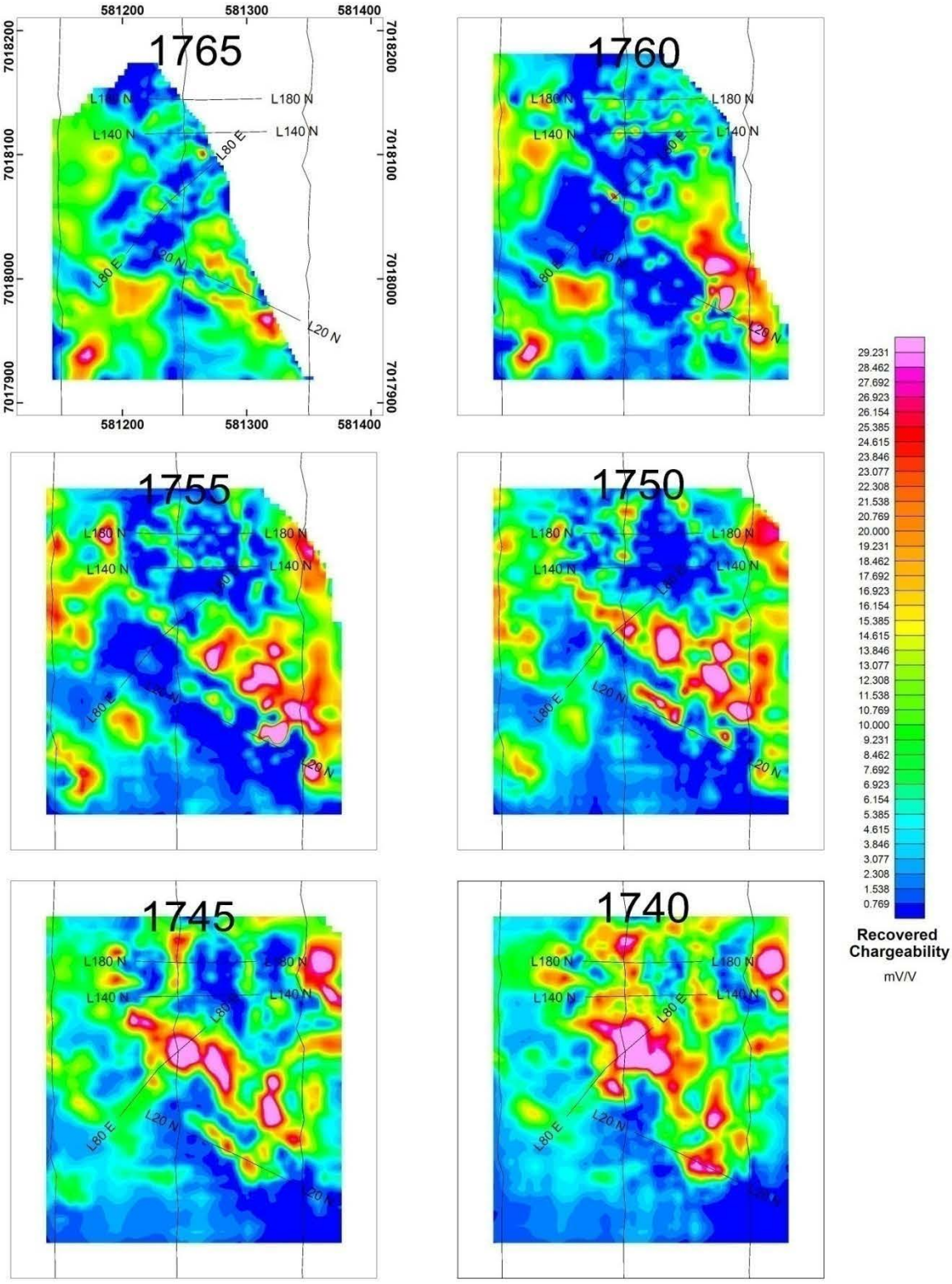

Figure 10: Overview of the detailed chargeability model. North is towards the top of the page.

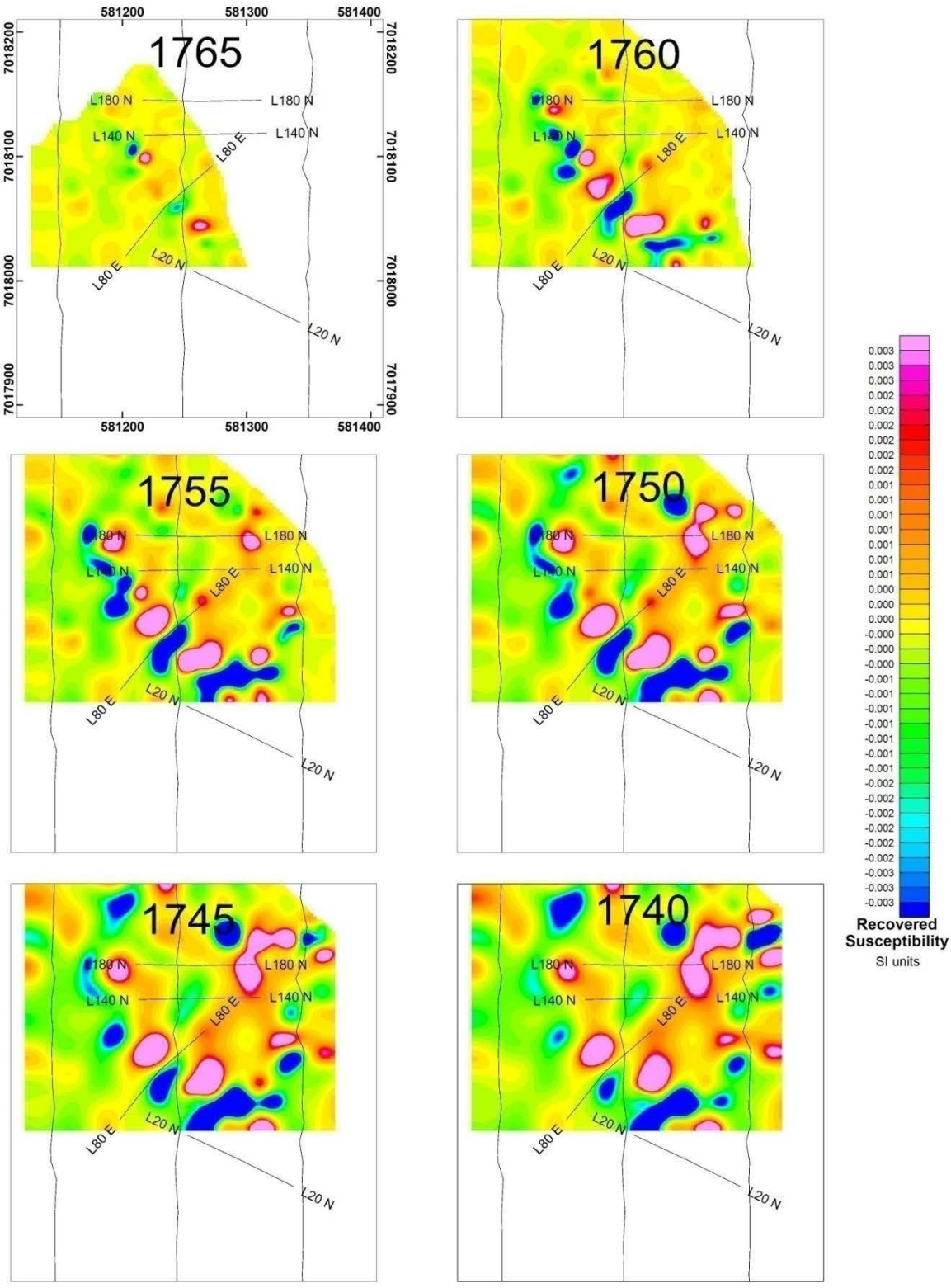

Figure 11: Plan view of the detailed magnetic models at different elevations. Hot colors indicate positive susceptibility and cold colors indicate negative susceptibility. North is towards the top of the page.

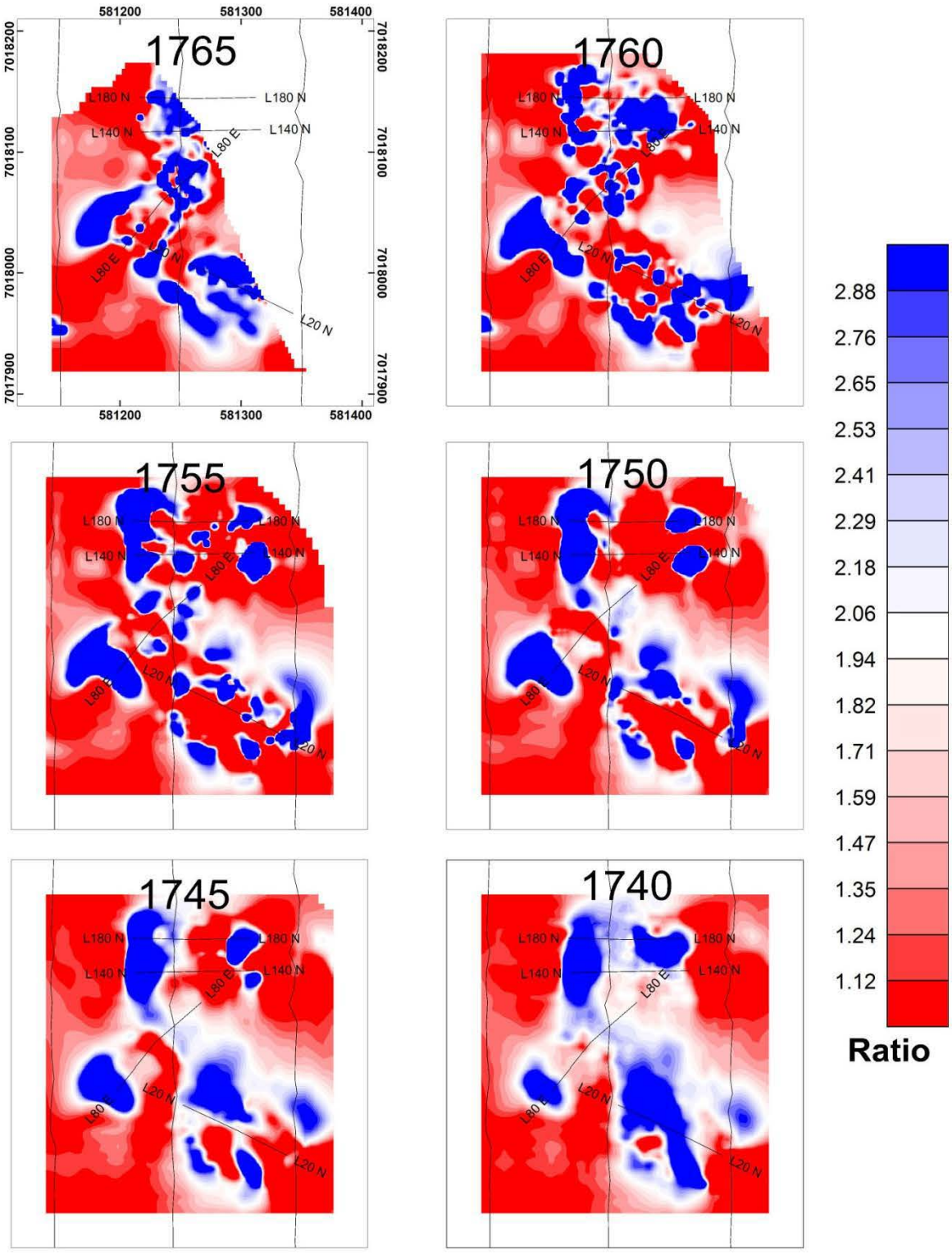

Figure 12: Overview of the ratio model. Red areas indicate areas of ratio less than 2 (felsic volcanic) and blue areas indicate areas of ratio higher than 2 (metasediment). Data is absent in the northeast corner at higher elevations because it is above the ground. North is towards the top of the page.

4.2 Comparison of models with drillholes and geochemistry

Detailed models are used for figures in this section.

VG Zone

A total of seven holes were drilled in the VG zone. All were collared in felsic volcanic, and six of seven intersected the metasediment unit around elevation 1740 m. The lithology change is consistent with transition between low and high ratio and chargeability, a decrease in conductivity and an increase in susceptibility (Figure 13). This is consistent with the rock physics results.

The best assay results show a reasonable correlation with moderate chargeability highs within the low chargeability felsic volcanic layer (Figure 13).

Ben Zone

The Ben zone (Figure 14) is approximately at the center of L80N as defined by the geochemical anomalies. This appears to be a structural focal point and there is a sharp contact in resistivity, susceptibility, chargeability and ratio here (Figure 8). The shift is from conductive rocks, presumably metasediment on the SW end of L80E transition into highly resistive.

SW Zone

The SW zone has one drillhole (Figure 15). There is a linear trend of geochemical anomalies here. Based on this single hole, the relationship between ratio, chargeability and lithology is inverted here, with the felsic volcanic rocks having a high ratio and chargeability. The linear trend of geochemical anomalies is oblique to the NW-SE fabric of the resistivity models. Chargeability is moderate to low on surface, with a few isolated anomalies north of L20E.

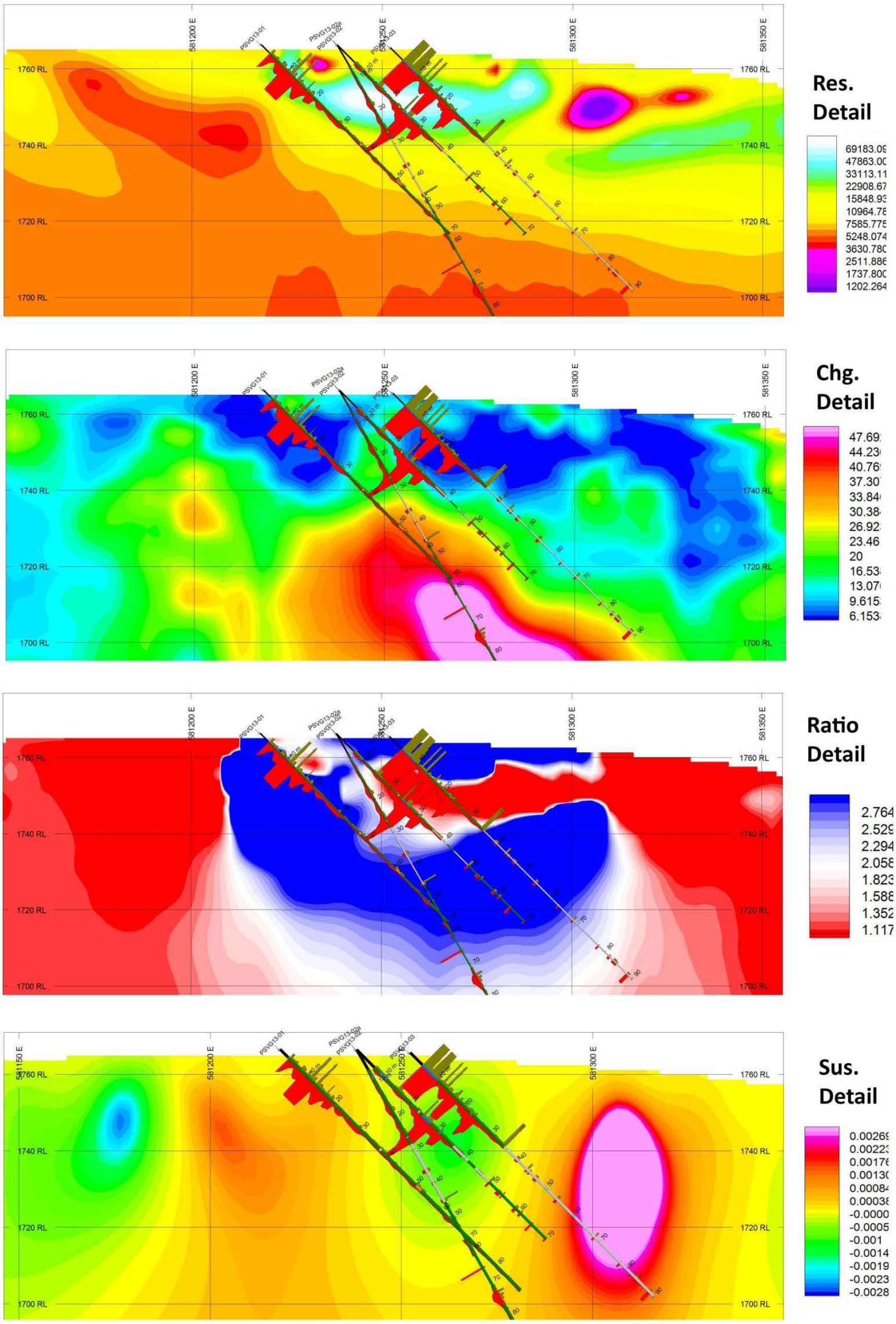

Figure 13: E-W cross-section through the center of the VG zone. Red profiles are arsenic values (linear, clipped at 200 ppm) and gold profiles (linear, clipped at 200 ppb) are gold values.

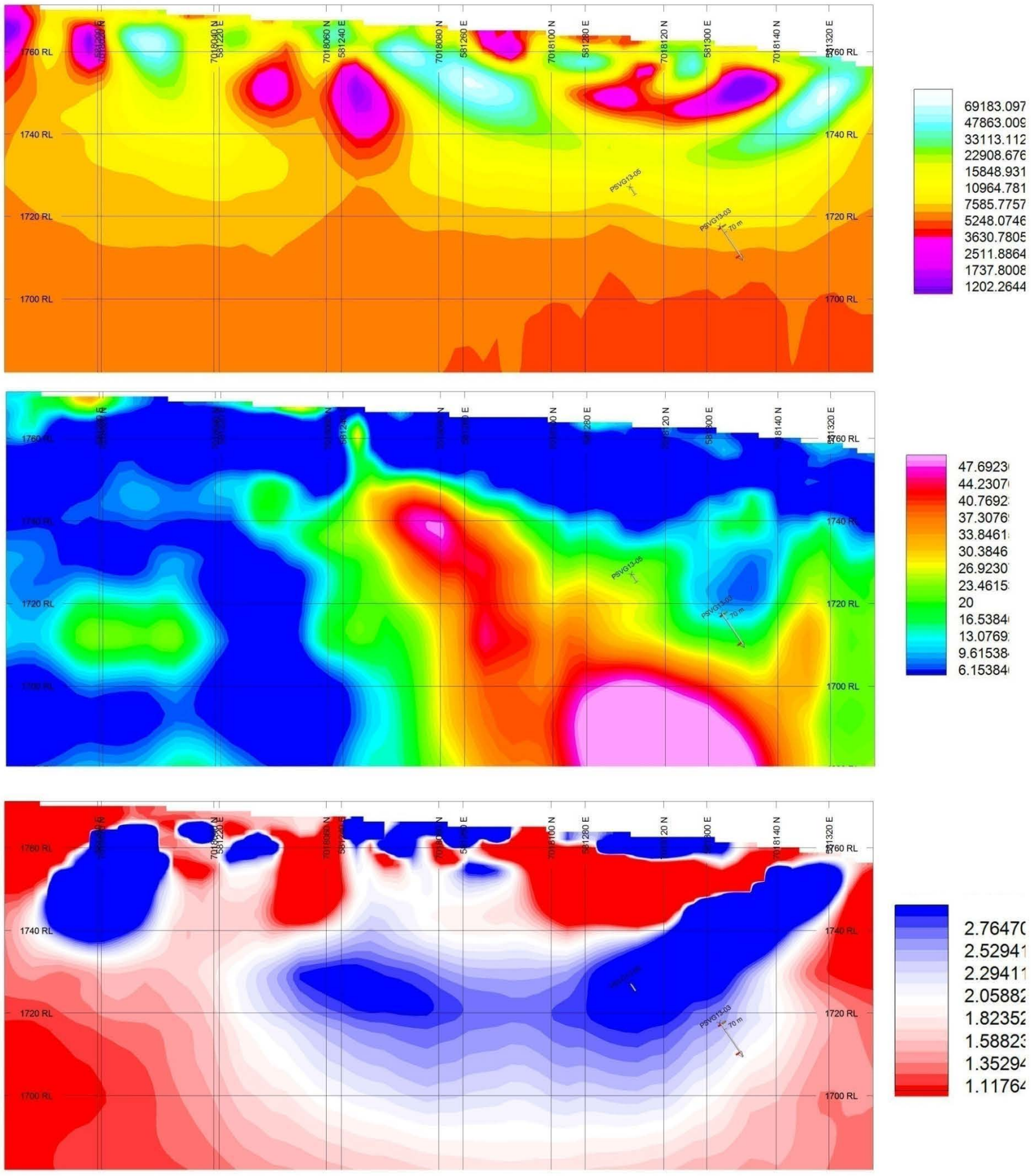

Figure 14: Cross-section through the Ben zone, under L80N. The right is towards the northeast and the left is to the southwest.

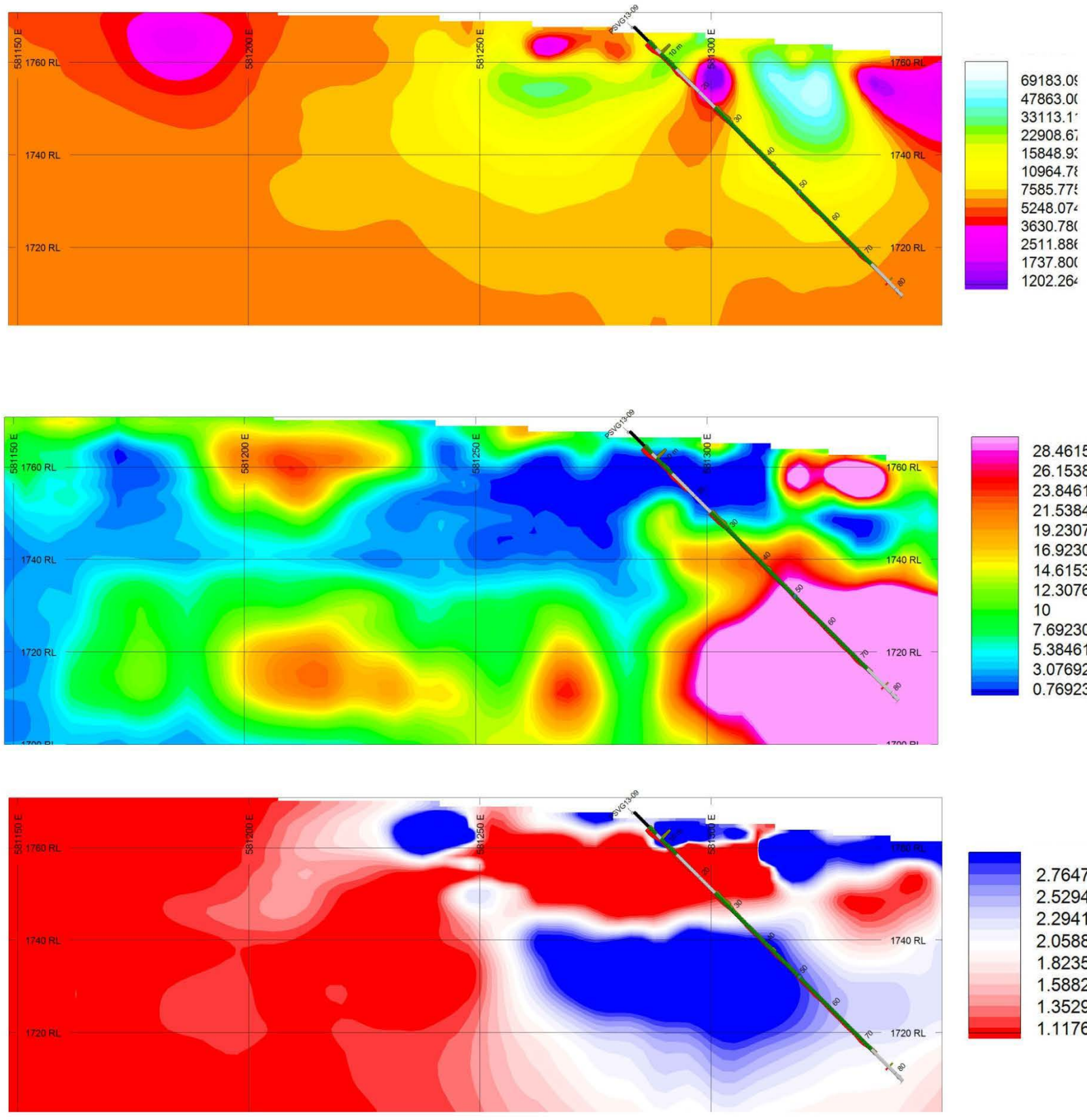

Figure 15: E-W section along the drill trace of DH13-09 in the SW zone. Red profiles are arsenic values (linear, clipped at 200 ppm) and gold profiles (linear, clipped at 200 ppb) are gold values.

4.3 Geochemical Correlation analysis

The recovered models were sampled along the drillholes and then cross correlation coefficients were calculated between the downhole geochemistry and the sampled geophysical models. (Table 2, Figure 16). Positive coefficients indicate a direct relationship while negative coefficients indicate an inverse relationship. Coefficients close to zero indicate little statistical correspondence between the datasets and coefficients close to one indicate almost perfect statistical correspondence.

Several trends are observed in the correlation analysis. The arsenic and gold are inversely correlated with the models when compared to the rest of the elements. The chargeability and detail susceptibility models have a positive correlation with most of the geochemistry, while the coarse susceptibility and resistivity models have a negative correlation. In real world terms this means that the gold and arsenic are associated with low chargeability, susceptibility and high resistivity, while the rest of the metals are related to high chargeability, high susceptibility and low resistivity.

This is consistent with the results of the rock physics which indicated similar relationships. The detailed chargeability model show the best correlation with the geochemistry, especially with chromium, magnesium, scandium, vanadium and zinc. This analysis confirms the relationship between geophysical properties and lithology from the rock physics. Calculating correlation within individual lithologies could give insight into mineralization within the units.

Table 2: Correlation between drillhole geochemistry and geophysical models.

	Res_coarse	Res_detail	Sus_coarse	Sus_detail	CHG_coarse	CHG_detail
As_ppm	0.09	0.32	0.05	-0.17	-0.31	-0.36
Au_3B_ppb	0.04	0.12	0.04	-0.08	-0.29	-0.31
Ba_ppm	-0.07	-0.08	-0.06	-0.01	0.04	0.08
Co_ppm	-0.07	-0.28	-0.08	0.20	0.28	0.31
Cr_ppm	-0.33	-0.40	-0.07	0.21	0.46	0.55
Cu_ppm	-0.05	-0.23	0.04	0.14	0.24	0.28
Fe_ppm	-0.13	-0.27	-0.08	0.18	0.26	0.29
La_ppm	-0.28	0.00	-0.03	0.04	-0.01	0.02
Mn_ppm	0.03	-0.20	-0.10	0.12	0.19	0.23
Mo_ppm	0.07	-0.08	-0.06	0.07	0.07	0.05
K_pct	-0.01	-0.22	-0.08	0.09	0.20	0.24
Ca_pct	0.28	-0.29	-0.12	0.15	0.22	0.26
Mg_pct	-0.18	-0.35	-0.11	0.29	0.33	0.40
Ni_ppm	-0.09	-0.30	-0.08	0.19	0.30	0.34
Pb_ppm	0.01	-0.08	0.01	-0.05	0.02	0.02
Sb_ppm	-0.21	-0.23	-0.15	0.21	0.09	0.15
Sc_ppm	-0.16	-0.33	-0.12	0.27	0.38	0.44
Sr_ppm	0.24	-0.28	-0.11	0.15	0.19	0.24
Th_ppm	-0.16	-0.12	-0.03	0.08	0.17	0.19
V_ppm	-0.20	-0.38	-0.04	0.22	0.38	0.43
Zn_ppm	-0.07	-0.26	-0.07	0.11	0.29	0.32

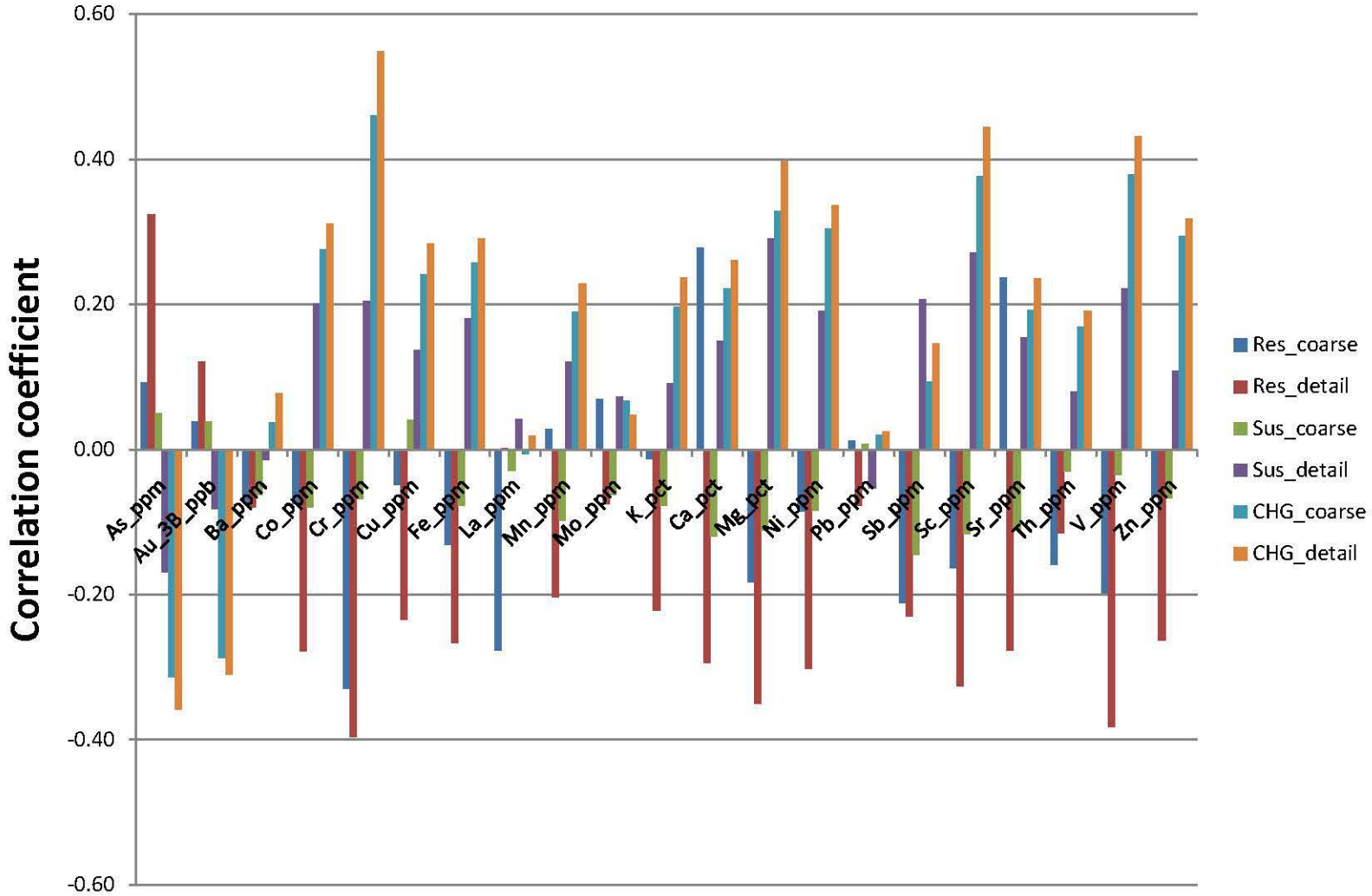

Figure 16: Graphical representation of the correlation between drillhole geochemistry and the recovered models.

4.4 Targeting using the models

Section 4.2 suggests the primary targets are relatively high chargeability zones within the felsic volcanics which are characterized by high resistivity, low chargeability and linear ratio below two.

A systematic approach was applied to the entire model in which grids are created at that have a value of 1 if the resistivity is above 10000 Ohm.m and the chargeability is between 10 and 30 mV/V. The results are shown in Figure 17 for the coarse grid. The analysis of the detailed grid is not shown here because the results were the same and it does not have the same coverage.

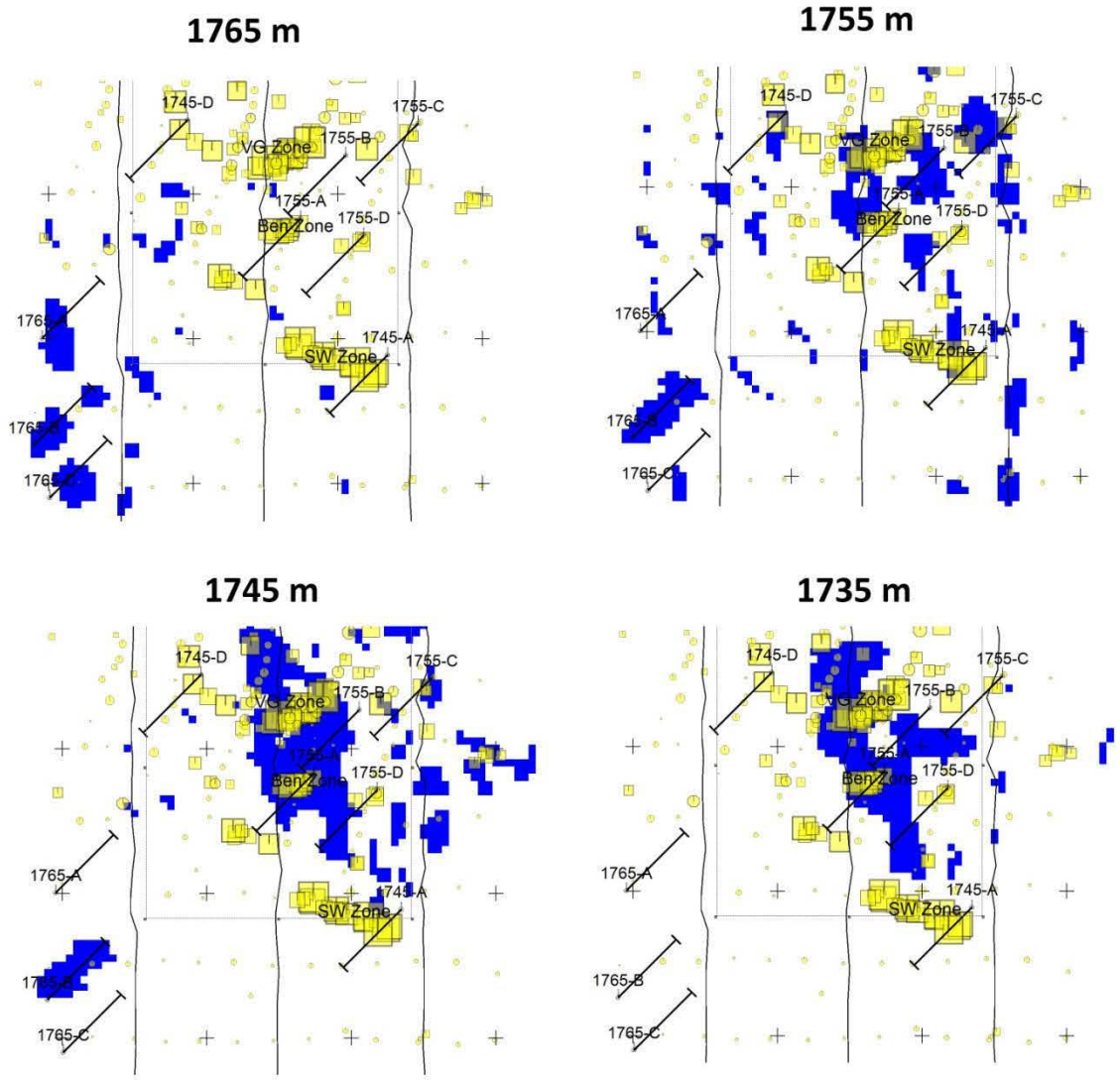

Figure 17: Plan view of the coarse model analysis showing prospective areas (blue) at different depth elevations. The yellow squares are gold values in surface rock samples and the yellow circles are gold values in soil samples along the drill traces indicate gold values. The recommended drillholes discussed in the recommendations are also plotted here.

4.5 Geological Interpretation

The dominantly NW-SE lineament in the first 50 m is interpreted to be a series of eroded folds (Figure 18). The folds alternate between conductive metasediment and highly resistive felsic volcanic. These folds are crosscut by a series of NE-SW structures which offset the folds . Dilation associated with this movement could have produced the fluid conduit which caused the

mineralization. The geochemistry (Figure 19) suggests that the gold is focused primarily in areas where offsets meet the resistive lineament of the fold, and secondarily along the contact between metasediment and felsic volcanic units.

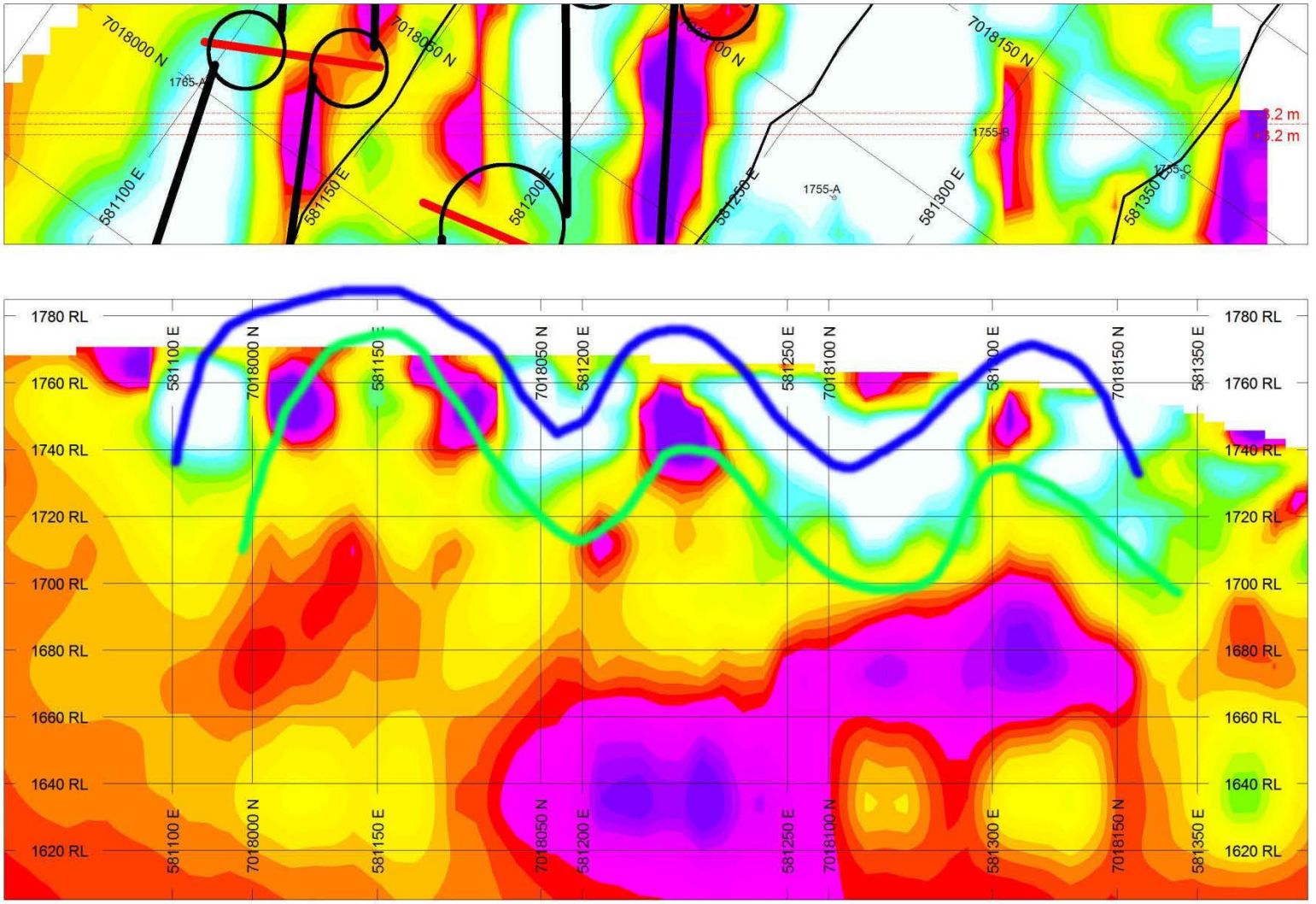

Figure 18: Cross section of the coarse resistivity model showing the interpreted fold structured. The blue lines are the resistivity folds and the green line is the conductive layer in the fold.

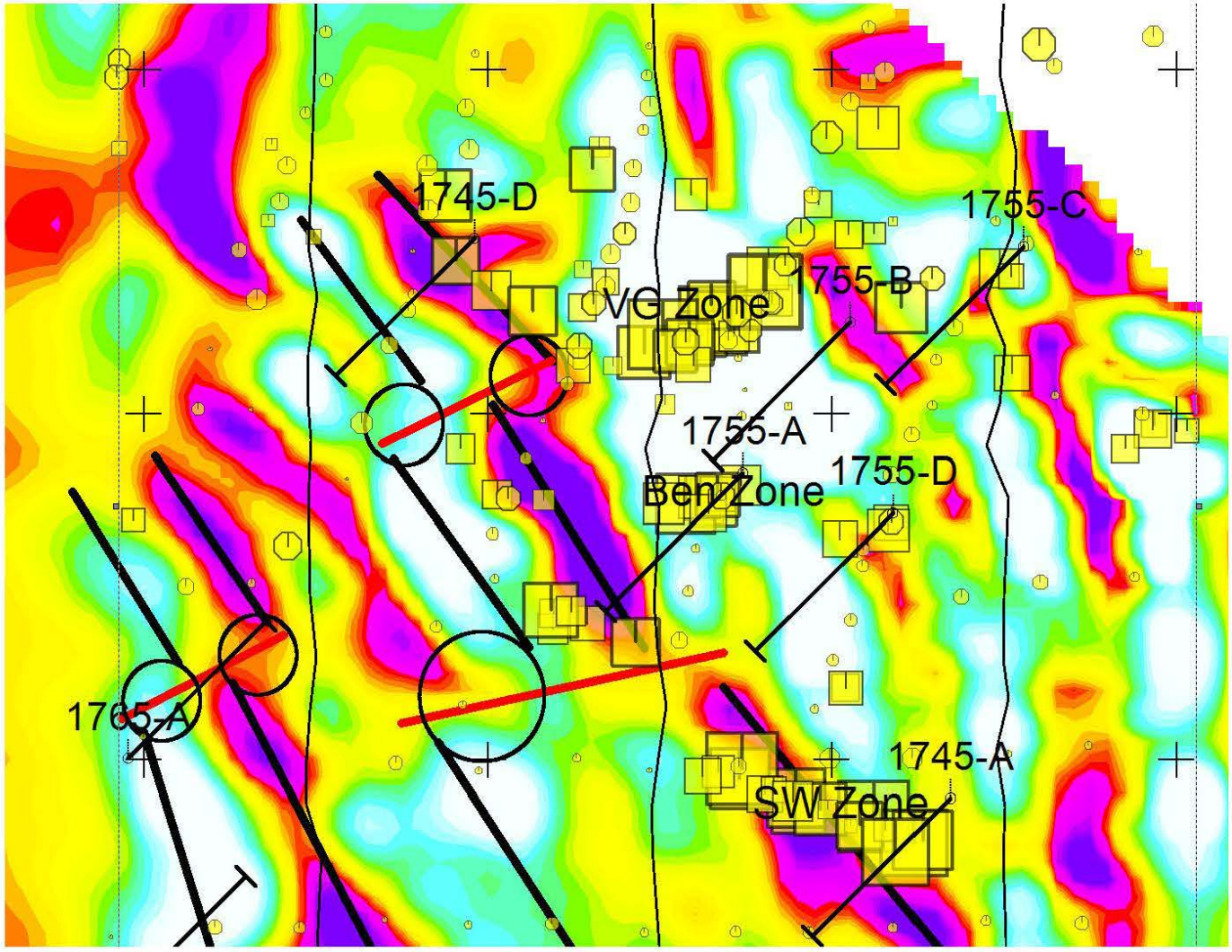

Figure 19: Plan view showing the relationship between the geochemistry, resistivity model and interpreted structures. Black lines indicate the dominant N-S resistivity lineaments and the red lines show the cross-cutting structure. Circles indicate possible dextral movement caused by the cross cutting structures. The yellow squares are gold values in surface rock samples and the yellow circles are gold values in soil samples along the drill traces indicate gold values.

5. RECOMMENDATIONS

Table 3 shows the list of targets generated in the analysis in section 4.4, and ranks them according to their geophysical and geochemical prospectivity and provides coordinates to the center of these. Table 4 lists the possible drillholes to test each anomaly. It is recommended that the drillholes locations should be revised by Goldstrike geologist prior to drilling based on intimate knowledge of ground conditions and detailed geology.

1765-A, B and C (Figure 20, Figure 21, Figure 22) test moderate chargeability highs within a linear resistivity high that is close to the surface (Figure 8). Data density here is relatively low and there are no geochemical anomalies. 1765-A is in line with the offset in the vicinity of VG zone. The offset at 1765-B is roughly in-line with the offset at the Ben zone. Anomaly 1765-C is not as structurally interesting, but it is a significant chargeability high within a highly resistive zone so it is included.

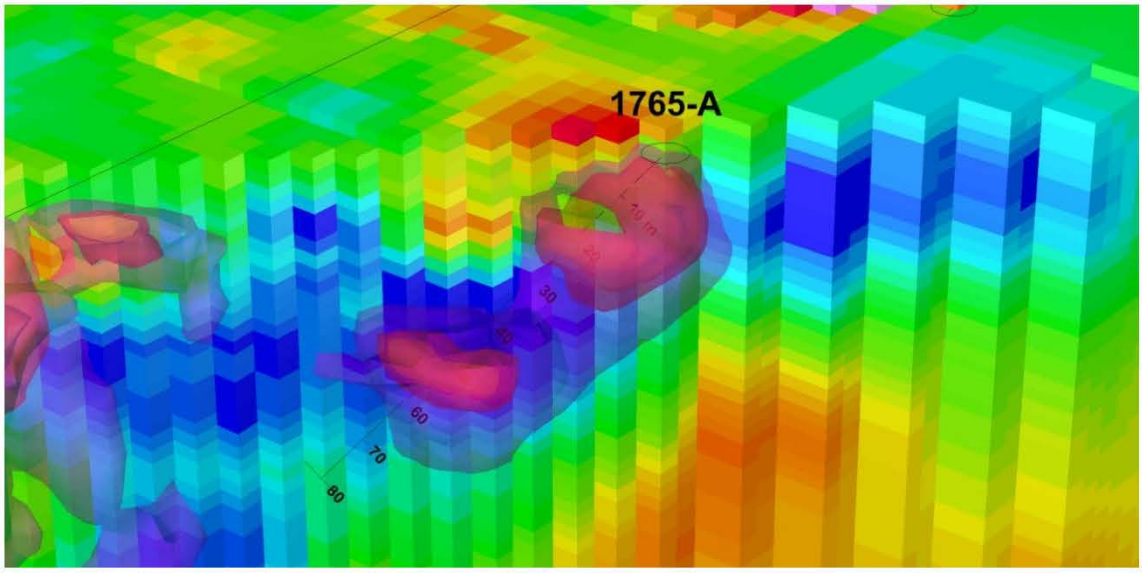

Figure 20: Inclined 3D view of target 1765-A and the recommended drillhole to test it.. The block model is chargeability and the isosurfaces are from the resistivity model. View is from the northwest.

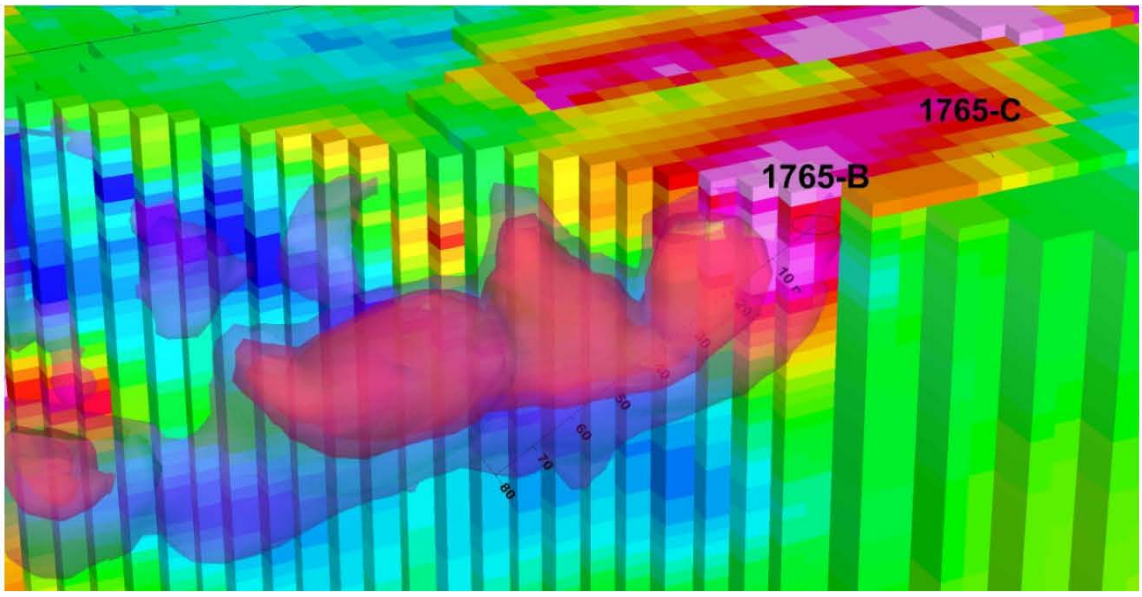

Figure 21: Inclined 3d view of target 1765-B and the recommended drillhole to test it.. The block model is chargeability and the isosurfaces are from the resistivity model. View is from the northwest

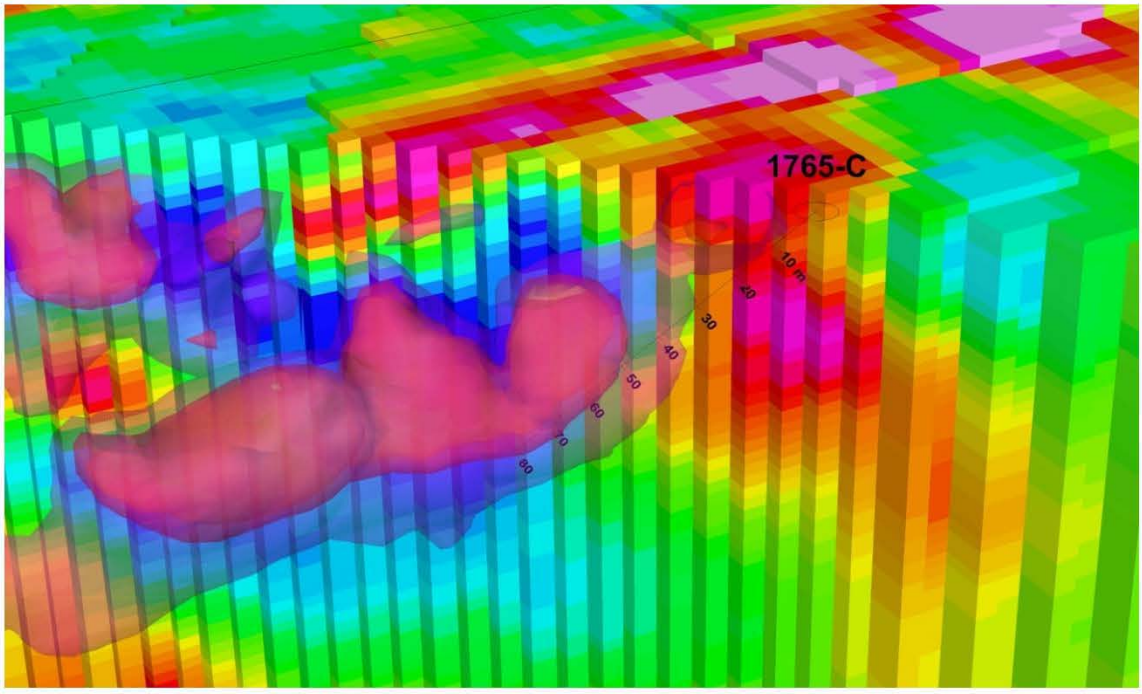

Figure 22: Inclined 3D view of target 1765-C and the recommended drillhole to test it.. The block model is chargeability and the isosurfaces are from the resistivity model. View is from the northwest.

1755-A (Figure 23) tests the Ben zone, and intersects a significant chargeability anomaly within the resistive layer. It is predicted go through mostly felsic volcanic rock until about 30-40 meters at which it will switch to metasediment. At this interface is the targeted chargeability anomaly.

1755-B and 1755-C (Figure 23) are in-line with the offset next to the VG zone, and have associated geochemical anomalies. 1755-C tests the northern extent of the deep, large conductive and chargeable unit, which is also tested by 1695-A.

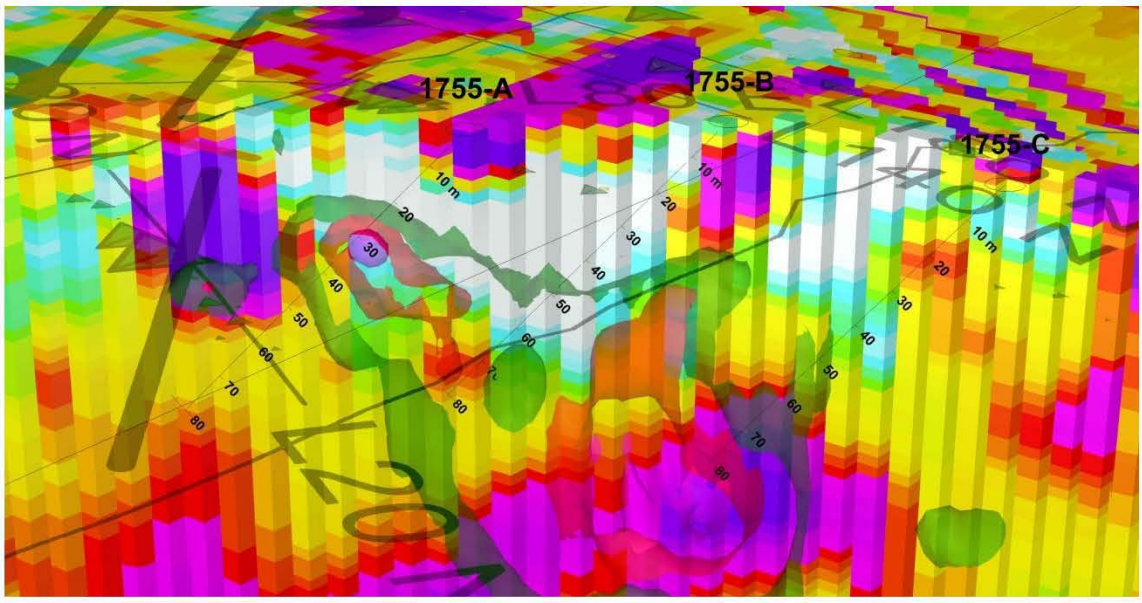

Figure 23: Inclined 3D view of anomalies 1 1745-A, B and C. The block model is the coarse resistivity and the isosurfaces are from the coarse chargeability. View is from the SE.

1755-D (Figure 24) tests the main resistivity anomaly in between Ben and VG at a location of relatively high chargeability. There is favourable geochemistry here and association with an offset.

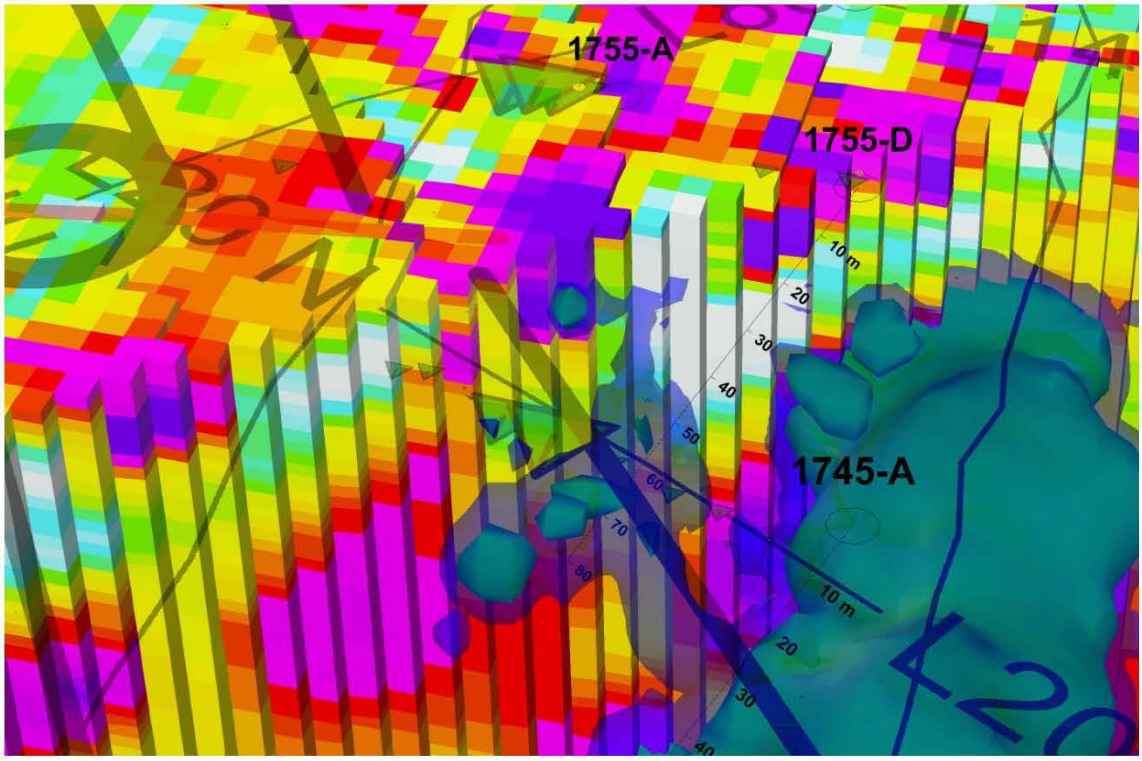

Figure 24: Inclined 3D view of target 1755-D and the drillhole that tests it. The block model is the coarse resistivity and the isosurfaces are from the coarse chargeability. View is from the SE.

1755-E tests the SW zone (Figure 25). It drills from the opposite direction as DH1309 and intersects the chargeability anomaly instead of going under it. The ratio and geochemistry are favourable here.

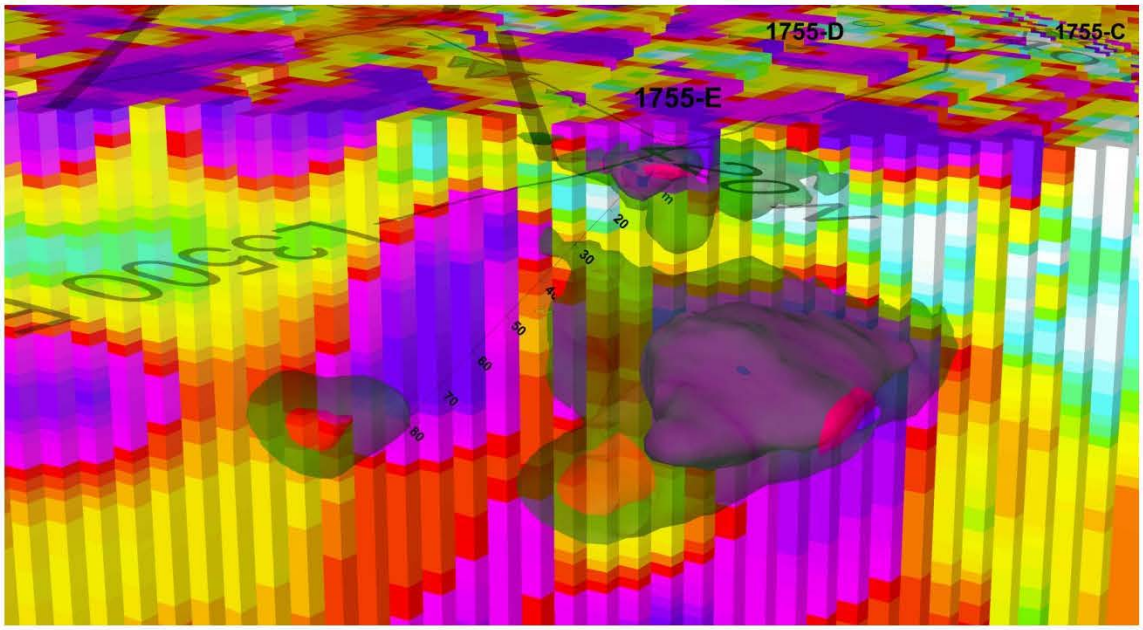

Figure 25: Inclined 3D view of target 1755-E and the drillhole that tests it. The block model is the coarse resistivity and the isosurfaces are from the coarse chargeability. View is from the SE.

Target 1745-A is a series of small chargeability anomalies within a wide resistive zone. The recommended drillhole test the best chargeability anomaly within this zone.

Target 1740-A test a chargeability target east of the holes VG zone (Figure 13).

Target 1695-A tests the large conductive and chargeability anomaly at depth beneath this L3500E.

Further coarse resistivity anda more detailed magnetic surveys are recommended in the area as well as more rock physics. The rock physics could come from a more thorough suite of samples to confirm the hypothesis, or from downhole surveys in the existing drillholes and in any future drillholes. The downhole surveys would provide a richer, in-situ and more continuous dataset, but requires an open hole. This would greatly help establish correlations between the lithology, geochemistry and the geophysical of the rocks on the hill.

As more geochemical and geological data becomes available, it is important to revisit the geophysical datasets. Once the geology is better established on the south plateau, it would be beneficial to create a geological model to use as a starting point for inversions. This is would lead to a more robust and realistic interpretation.

Table 3: Summary of targets and their priority.

Target ID	Detail Analysis	Ratio	Geochemistry	Structural	Priority	Comment
1765-A	N/A	N/A	none	Good	3	Low priority target on the west side of L1500E
1765-B	N/A	N/A	none	Moderate	3	Low priority target on the west side of L1500E
1765-C	N/A	N/A	none	Poor	3	Low priority target on the west side of L1500E
1755-A	Moderate	Moderate	Good	Good	1	North part of this anomaly has been drilled (VG zone) south part of this target is the Ben zone, highly prospective.
1755-B	Poor	Good	Good	Good	1	Separated from 1755-A by a low resistivity zone.
1755-C	Good	Good	moderate	Good	2	Separated for 1755-A by a low resistivity zone.
1755-D	Good	moderate	low	Moderate	2	In the moderate chargeability anomaly within the high resistivity trend that connects the SW zone and the Ben zone
1755-E	Moderate	Moderate	Good	Moderate	1	Good target, drillhole appears to have missed the target
1745-A	N/A	Good	moderate	Good	3	Wide area of high resistivity with a few small chargeability anomalies. A couple small geochem anomalies here.
1740-A	Good	Poor	Moderate	Good	1	Target at elevation 1740, not shown in map. Chargeability high within a resistivity low.
1695-A	n/A	n/A	n/A	n/A	3	The large conductive and chargeable unit at depth. Low priority target, but might be worth examining.

Table 4: Recommended drill holes to test the above anomalies

HOLEID	East	North	Elev	Dip	Azimuth	TD
1765-A	581095.6	7018000	1770.82	-45	45	80
1765-B	581089.9	7017926	1773.03	-45	45	80
1765-C	581100.8	7017890	1774.07	-45	45	80
1755-A	581274.2	7018083	1765.61	-45	225	80
1755-B	581305.5	7018127	1762.49	-45	225	80
1755-C	581355.7	7018149	1754.18	-45	225	80
1755-D	581317.8	7018071	1762.31	-45	225	80
1755-E	581334.5	7017989	1763.32	-45	225	80
1745-A	581196	7018151	1765.56	-45	225	80
1740-A	581320	7018150	1759.3	-45	225	80
1695-A	581340	7018067	1760.2	-90	225	125

6. Conclusions

The rock physics show that the target felsic volcanic units are moderately to highly resistive (with some exceptions) and have a distinct moderate IP response. The metasediment units in the area have a variable response, from a conductive and extreme chargeable shale to amoderately resistive, non-chargeable shale. The rock physics introduce a new variable to differentiate between the metasediment and the felsic volcanic units on the basis of the character of their decay curve. As the understanding of geology in the area increases, this ratio could be a useful tool for identifying highly prospective areas.

The geophysical surveys in the VG zone of the South Plateau show the area to be structurally complex with a high variability in resistivity and chargeability. The dominantly NW-SE lineament in the first 50 m is interpreted to be a series of eroded folds (Figure 18). The folds alternate between conductive metasediment and highly resistive felsic volcanic. These folds are crosscut by a series of NE-SW structures which offset the folds . Dilation associated with this movement could have produced the fluid conduit causing the mineralization. The geochemistry (Figure 19) suggests that the gold is focused primarily in areas where offsets meet the resistive lineament of the fold, and secondarily along the contact between metasediment and felsic volcanic units.

Correlation between the models and the drillhole geochemistry was calculated (Figure 16), and the results showed that the gold and arsenic are associated with low chargeability, susceptibility and high resistivity, while the rest of the metals are related to high chargeability, high susceptibility and low resistivity. This is consistent with the rock physics observation of 2 main rock types in the area. This analysis describes confirms the broad association between lithology and geophysical properties, but does not capture association between the mineralization and moderate chargeability highs.

A systematic approach is used to analyze the data for further exploration. Areas of high resistivity and moderate chargeability are outlined and ranked according to their geophysical and geochemical properties. A total of nine anomalies are found using this analysis, some corresponding to existing drillholes/geochemistry and other are new areas of exploration.

Recommendations for further work include drilling, more resistivity/ IP surveys, magnetic surveys, and downhole geophysical surveys. As new data is gathered on south plateau, the geophysical interpretation should be revisited.

7. PRODUCTS

\Final Models	Final RESIP models in geosoft voxel and ASCII XYZ format
\Predicted vs Observed	Figures comparing the predicted and observed data from the RESIP inversions
\3D Maps	3D PDF, 3D geosoft map and 3D DXF
\Plan Grids	Geosoft grids of the recovered models at various levels
\Figures\	Full resolution versions of selected figures in the report, in jpg or pdf format

Respectfully Submitted,

Louis Rosenthal

Dave Hildes

AURORA GEOSCIENCES

PHYSICAL PROPERTY LAB REPORT

Sample #: 1

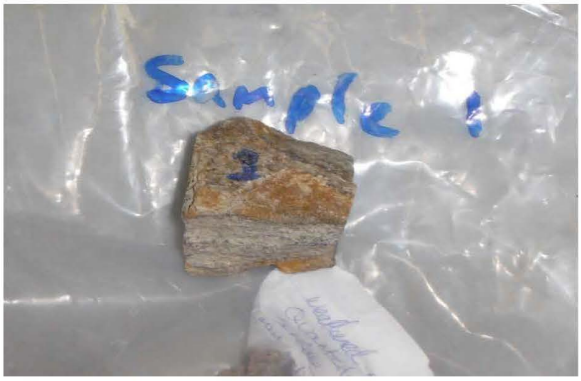

Rock Sample Description

Rock type	Weathered Altered Quartzite
Comment	Found at the surface near mineralized zone

Physical properties of the Rock Sample:

Porosity (%)	8.54
Specific Gravity (g/cm3)	2.51
Magnetic Susceptibility (X 10e3 SI Units)	0.028888889
Resistivity Mean (Ohm - m)	3679.38
Resistivity Dev (Ohm - m)	80.13
IP Response (mV/V)	6.90
IP Response Dev (mV/V)	0.56
Temperature at which specific gravity was measured (C)	18

Notes: Remanent Mag was measured in six directions.

Measured by:

Andre Lebel

October 7, 2014

Date

AURORA GEOSCIENCES

PHYSICAL PROPERTY LAB REPORT

Sample #: 2

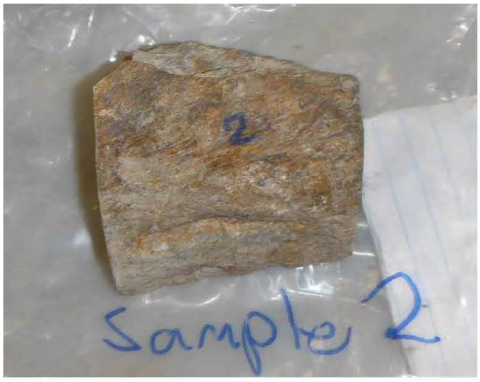

Rock Sample Description

Rock type	Fault vein
Comment	Typical fault vien material, classic target, good stuff where there is none of this ?

Physical properties of the Rock Sample:

Porosity (%)	2.91
Specific Gravity (g/cm3)	2.61
Magnetic Susceptibility (X 10e3 SI Units)	0.017
Resistivity Mean (Ohm - m)	5208.07
Resistivity Dev (Ohm - m)	79.87
IP Response (mV/V)	9.57
IP Response Dev (mV/V)	0.31
Temperature at which specific gravity was measured (C)	18

Notes: Remanent Mag was measured in six directions.

Measured by: Andre Lebel

October 7, 2014

AURORA GEOSCIENCES

PHYSICAL PROPERTY LAB REPORT

Sample #: 3

Rock Sample Description

Rock type	Altered sediments / Shale / with alteration minerals
Comment	Minerals likely Andalocite typically along block faults

Physical properties of the Rock Sample:

Porosity (%)	1.52
Specific Gravity (g/cm3)	2.79
Magnetic Susceptibility (X 10e3 SI Units)	0.2131
Resistivity Mean (Ohm - m)	1261.67
Resistivity Dev (Ohm - m)	157.91
IP Response (mV/V)	3.37
IP Response Dev (mV/V)	0.59
Temperature at which specific gravity was measured (C)	18

Notes: Remanent Mag was measured in six directions.

Measured by: Andre Lebel

October 7, 2014

AURORA GEOSCIENCES

PHYSICAL PROPERTY LAB REPORT

Sample #: 4

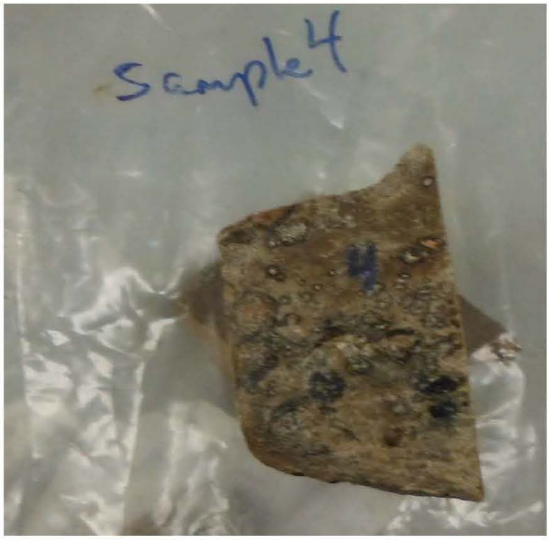

Rock Sample Description

Rock type	Quartzite with interbeds of sulphides
Comment	Sulphide percentage can vary wildly some dispute as to the posibility of felsic volcanicsas seen in the logs

Physical properties of the Rock Sample:

Porosity (%)	1.47
Specific Gravity (g/cm3)	2.60
Magnetic Susceptibility (X 10e3 SI Units)	0.038
Resistivity Mean (Ohm - m)	3349.19
Resistivity Dev (Ohm - m)	59.32
IP Response (mV/V)	5.20
IP Response Dev (mV/V)	0.40
Temperature at which specific gravity was measured (C)	18

Notes: Remanent Mag was measured in six directions.

Measured by:

Andre Lebel

October 7, 2014

Date

AURORA GEOSCIENCES

PHYSICAL PROPERTY LAB REPORT

Sample #: 5

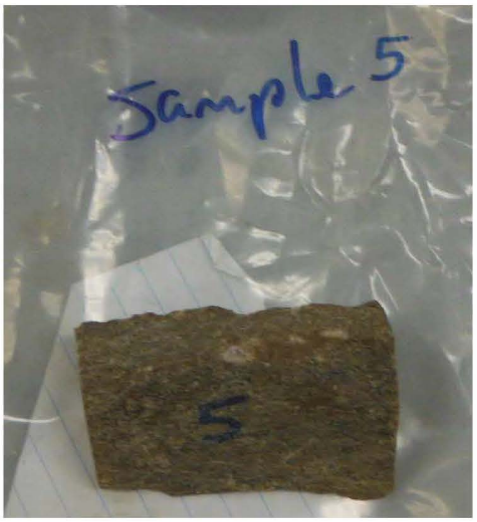

Rock Sample Description

Rock type	Quartzite
Comment	Near faults thjat are potentially mineralized , and show some schistoscity, Typcal of suvey area

Physical properties of the Rock Sample:

Porosity (%)	2.55
Specific Gravity (g/cm3)	2.64
Magnetic Susceptibility (X 10e3 SI Units)	0.021
Resistivity Mean (Ohm - m)	12641.49
Resistivity Dev (Ohm - m)	136.75
IP Response (mV/V)	9.33
IP Response Dev (mV/V)	0.12
Temperature at which specific gravity was measured (C)	18

Notes: Remanent Mag was measured in six directions.

Measured by:

Andre Lebel

October 7, 2014

Date

AURORA GEOSCIENCES

PHYSICAL PROPERTY LAB REPORT

Sample #: 6

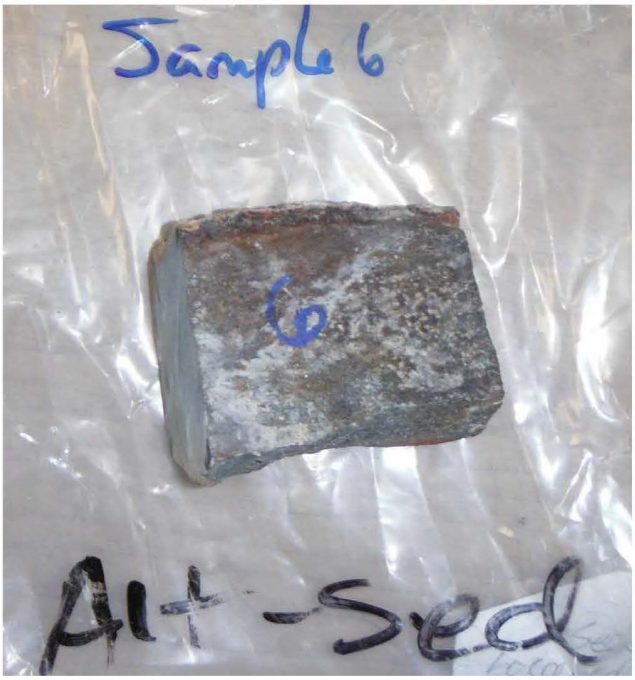

Rock Sample Description

Rock type	Altered Sediments
Comment	Located Close to Mt-Armstrong intrusion, so contact alteration typical of

Physical properties of the Rock Sample:

Porosity (%)	1.86
Specific Gravity (g/cm3)	2.73
Magnetic Susceptibility (X 10e3 SI Units)	0.067
Resistivity Mean (Ohm - m)	9742.63
Resistivity Dev (Ohm - m)	440.27
IP Response (mV/V)	4.75
IP Response Dev (mV/V)	0.35
Koenigsberger ratio (Q)	0.77
Temperature at which specific gravity was measured (C)	18

Notes: Remanent Mag was measured in six directions.

Measured by:

Andre Lebel

October 7, 2014

Date

AURORA GEOSCIENCES

PHYSICAL PROPERTY LAB REPORT

Sample #: 7

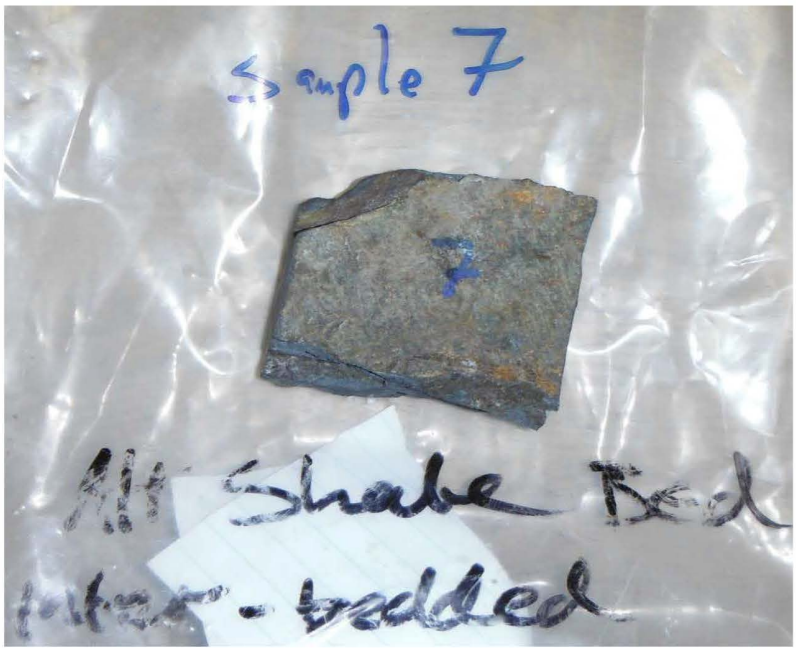

Rock Sample Description

Rock type	Altered Shale, inter-bedded
Comment	Shale beds typical intercepts of various percentages of sulphides, shalow dipping to the south?

Physical properties of the Rock Sample:

Porosity (%)	0.76
Specific Gravity (g/cm3)	2.73
Magnetic Susceptibility (X 10e3 SI Units)	0.029
Resistivity Mean (Ohm - m)	1063.79
Resistivity Dev (Ohm - m)	9.76
IP Response (mV/V)	93.43
IP Response Dev (mV/V)	2.82
Temperature at which specific gravity was measured (C)	18

Notes: Remanent Mag was measured in six directions.

Measured by:

Andre Lebel

October 7, 2014

Date

AURORA GEOSCIENCES

PHYSICAL PROPERTY LAB REPORT

Sample #: 8

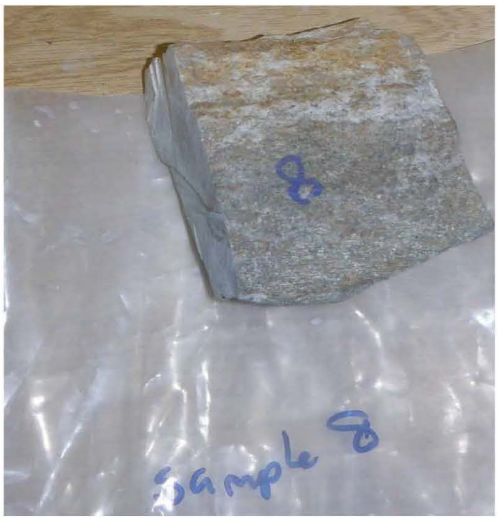

Rock Sample Description

Rock type	Quartzite
Comment	Typical less altered quartzite

Physical properties of the Rock Sample:

Porosity (%)	1.47
Specific Gravity (g/cm3)	2.61
Magnetic Susceptibility (X 10e3 SI Units)	0.042
Resistivity Mean (Ohm - m)	7498.41
Resistivity Dev (Ohm - m)	9.68
IP Response (mV/V)	8.17
IP Response Dev (mV/V)	0.21
Koenigsberger ratio (Q)	0.21
Temperature at which specific gravity was measured (C)	18

Notes: Remanent Mag was measured in six directions.

Measured by:

Andre Lebel

October 7, 2014

Date

AURORA GEOSCIENCES

PHYSICAL PROPERTY LAB REPORT

Sample #: 13-03-01 21.5 - 22

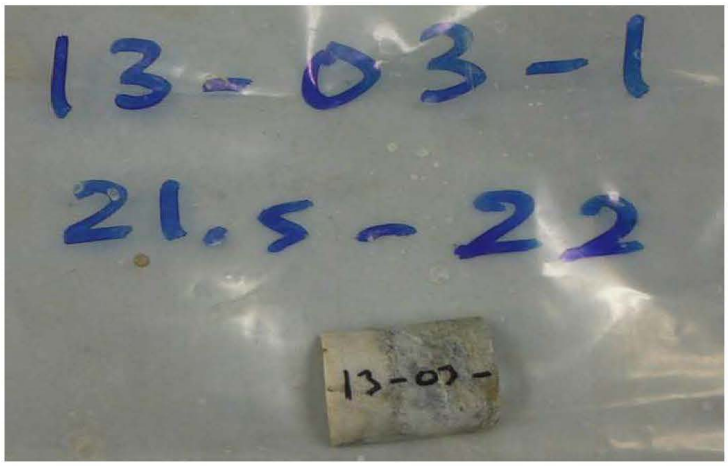

Rock Sample Description

Rock type	
Comment	

Physical properties of the Rock Sample:

Porosity (%)	1.06
Specific Gravity (g/cm3)	2.64
Magnetic Susceptibility (X 10e3 SI Units)	0.03
Resistivity Mean (Ohm - m)	931.33
Resistivity Dev (Ohm - m)	45.33
IP Response (mV/V)	4.73
IP Response Dev (mV/V)	0.06
Temperature at which specific gravity was measured (C)	18

Notes: Remanent Mag was measured in six directions.

Measured by:

Andre Lebel

October 7, 2014

Date

AURORA GEOSCIENCES

PHYSICAL PROPERTY LAB REPORT

Sample #: 13-03-2 34 -34.5

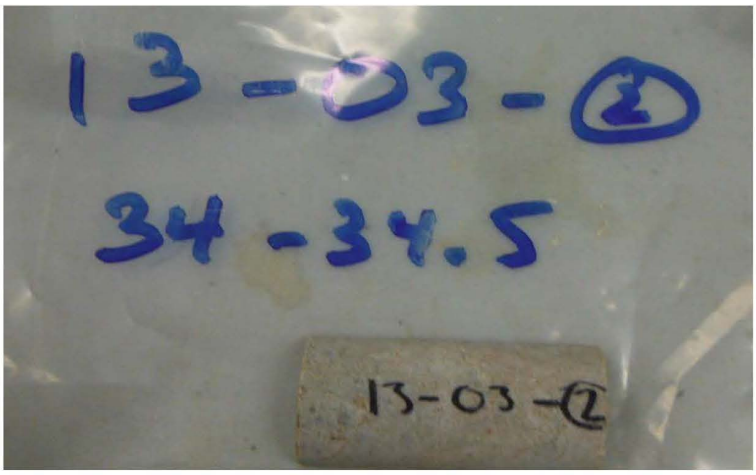

Rock Sample Description

Rock type	
Comment	

Physical properties of the Rock Sample:

Porosity (%)	1.23
Specific Gravity (g/cm3)	2.64
Magnetic Susceptibility (X 10e3 SI Units)	0.018
Resistivity Mean (Ohm - m)	685.13
Resistivity Dev (Ohm - m)	38.42
IP Response (mV/V)	5.13
IP Response Dev (mV/V)	0.25
Temperature at which specific gravity was measured (C)	18

Notes: Remanent Mag was measured in six directions.

Measured by:

Andre Lebel

October 7, 2014

Date

AURORA GEOSCIENCES

PHYSICAL PROPERTY LAB REPORT

Sample #:13-02-A-1 43

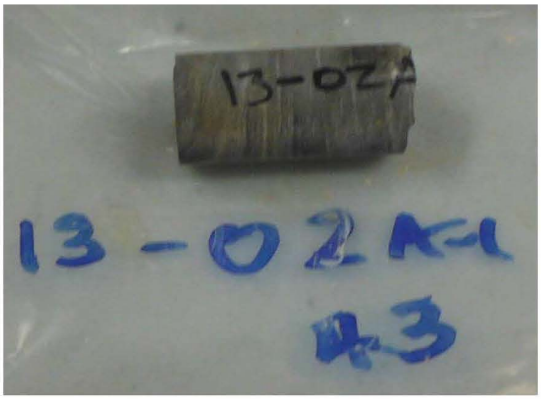

Rock Sample Description

Rock type	
Comment	

Physical properties of the Rock Sample:

Porosity (%)	0.72
Specific Gravity (g/cm3)	2.83
Magnetic Susceptibility (X 10e3 SI Units)	0.1175
Resistivity Mean (Ohm - m)	18382.21
Resistivity Dev (Ohm - m)	198.65
IP Response (mV/V)	4.70
IP Response Dev (mV/V)	0.42
Koenigsberger ratio (Q)	0.06
Temperature at which specific gravity was measured (C)	18

Notes: Remanent Mag was measured in six directions.

Measured by: Andre Lebel

October 7, 2014
Date

AURORA GEOSCIENCES

PHYSICAL PROPERTY LAB REPORT

Sample #: 13-03-03 41- 42

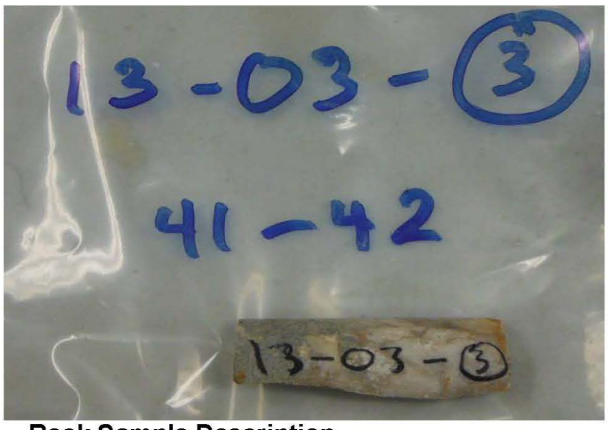

Rock Sample Description

Rock type	
Comment	

Physical properties of the Rock Sample:

Porosity (%)	1.14
Specific Gravity (g/cm3)	2.65
Magnetic Susceptibility (X 10e3 SI Units)	0.022
Resistivity Mean (Ohm - m)	785.06
Resistivity Dev (Ohm - m)	107.78
IP Response (mV/V)	5.15
IP Response Dev (mV/V)	0.07
Temperature at which specific gravity was measured (C)	18

Notes: Remanent Mag was measured in six directions.

Measured by: Andre Lebel

October 7, 2014
Date

AURORA GEOSCIENCES

PHYSICAL PROPERTY LAB REPORT

Sample #: 13-02-2A 182-183

Rock Sample Description

Rock type	
Comment	

Physical properties of the Rock Sample:

Porosity (%)	0.61
Specific Gravity (g/cm3)	2.67
Magnetic Susceptibility (X 10e3 SI Units)	0.086
Resistivity Mean (Ohm - m)	7466.87
Resistivity Dev (Ohm - m)	334.36
IP Response (mV/V)	6.20
IP Response Dev (mV/V)	0.14
Koenigsberger ratio (Q)	1.09
Temperature at which specific gravity was measured (C)	18

Notes: Remanent Mag was measured in six directions.

Measured by: Andre Lebel

October 7, 2014
Date

DENSIMETER

Sample ID

Calibration:

Time:

Lab Temp: 17 Solution conductivity with big samples

Water Temp: 17

Solution Conductivity (mmohm):

	Proper	Experimental
Mass:	0.00g	0.00g

Temp: 21 4 C (compensating) (@ 4 C H20 = 1g/cm^3)

Sample ID	1		
Width (cm)			
Length (cm)			
Height (cm)			
Volume (cm^3)	14.63		
Mass (dry, g)	35.53		
Mass (saturated,g)	36.78		
Mass in solution	22.14		
Specific Gravity (g/cm^3)	2.509		
Porosity (%):	8.544087491		
Porosity average (%):	8.544087491		

Sample ID	6		
Width (cm)			
Length (cm)			
Height (cm)			
Volume (cm^3)	9.654		
Mass (dry, g)	26.19		
Mass (saturated,g)	26.37		
Mass in solution	16.72		
Specific Gravity (g/cm^3)	2.731		
Porosity (%):	1.864512119		
Porosity average (%):	1.864512119		

Sample ID	13-03-1 21.5-22	
Width (cm)		
Length (cm)		
Height (cm)		
Volume (cm^3)	19.835	
Mass (dry, g)	52.24	
Mass (saturated,g)	52.45	
Mass in solution	32.63	
Specific Gravity (g/cm^3)	2.64	
Porosity (%):	1.05873456	
Porosity average (%):	1.05873456	

Sample ID	13-03-2 34-34.5	
Width (cm)		
Length (cm)		
Height (cm)		
Volume (cm^3)	32.401	
Mass (dry, g)	85.07	
Mass (saturated,g)	85.47	
Mass in solution	33.09	
Specific Gravity (g/cm^3)	2.638	
Porosity (%):	1.234529798	
Porosity average (%):	1.234529798	

Sample ID	7		
Width (cm)			
Length (cm)			
Height (cm)			
Volume (cm^3)	7.878		
Mass (dry, g)	21.47		

Mass (saturated,g)	21.53
Mass in solution	13.66
Specific Gravity (g/cm^3)	2.733
Porosity (%):	0.761614623
Porosity average (%):	0.761614623

Sample ID	2		
Width (cm)			
Length (cm)			
Height (cm)			
Volume (cm^3)	33.328		
Mass (dry, g)	86.08		
Mass (saturated,g)	87.05		
Mass in solution	53.58		
Specific Gravity (g/cm^3)	2.614		
Porosity (%):	2.910465675		
Porosity average (%):	2.910465675		

Sample ID	5		
Width (cm)			
Length (cm)			
Height (cm)			
Volume (cm^3)	12.965		
Mass (dry, g)	33.89		
Mass (saturated,g)	34.22		
Mass in solution	21.25		
Specific Gravity (g/cm^3)	2.639		
Porosity (%):	2.545314308		
Porosity average (%):	2.545314308		

Sample ID	13-03-3 41-42		
Width (cm)			

Length (cm)	
Height (cm)	
Volume (cm^3)	23.635
Mass (dry, g)	62.28
Mass (saturated,g)	62.55
Mass in solution	38.94
Specific Gravity (g/cm^3)	2.647
Porosity (%):	1.142373598
Porosity average (%):	1.142373598

Sample ID	3		
Width (cm)			
Length (cm)			
Height (cm)			
Volume (cm^3)	30.27		
Mass (dry, g)	84.02		
Mass (saturated,g)	84.48		
Mass in solution	54.24		
Specific Gravity (g/cm^3)	2.791		
Porosity (%):	1.519656426		
Porosity average (%):	1.519656426		

Sample ID	13-02A2 182-183	
Width (cm)		
Length (cm)		
Height (cm)		
Volume (cm^3)	11.366	
Mass (dry, g)	30.301	
Mass (saturated,g)	30.37	
Mass in solution	19.01	
Specific Gravity (g/cm^3)	2.672	
Porosity (%):	0.607073729	

Porosity average (%):	0.607073729

Sample ID	13-02-A1 43		
Width (cm)			
Length (cm)			
Height (cm)			
Volume (cm^3)	23.766		
Mass (dry, g)	67.07		
Mass (saturated,g)	67.24		
Mass in solution	43.54		
Specific Gravity (g/cm^3)	2.829		
Porosity (%):	0.715307582		
Porosity average (%):	0.715307582		

Sample ID	8		
Width (cm)			
Length (cm)			
Height (cm)			
Volume (cm^3)	27.265		
Mass (dry, g)	71.62		
Mass (saturated,g)	72.02		
Mass in solution	44.78		
Specific Gravity (g/cm^3)	2.614		
Porosity (%):	1.46708234		
Porosity average (%):	1.46708234		

Sample ID	4		
Width (cm)			
Length (cm)			
Height (cm)			

Volume (cm^3)	17.188
Mass (dry, g)	44.48
Mass (saturated,g)	44.74
Mass in solution	27.56
Specific Gravity (g/cm^3)	2.603
Porosity (%):	1.46708234
Porosity average (%):	1.46708234

Sample #	1
1	0.03
2	0.01
3	0.03
4	0.03
5	0.03
6	0.04
7	0.03
8	0.03
9	0.03
10	
Average	0.028888889

Sample #	2
1	0
2	0
3	0.05
4	-0.02
5	0.05
6	0.02
7	0.01
8	0.01
9	0.03
10	0.02
Average	0.017

Sample #	3
1	0.12
2	0.25
3	0.14
4	0.111
5	0.1
6	0.15
7	0.2
8	0.16
9	0.46
10	0.44
Average	0.2131

Sample #	4

1	0.02
2	0.02
3	0.02
4	0.01
5	0.03
6	0.2
7	0.01
8	0.02
9	0.02
10	0.03
Average	0.038

Sample #	5
1	0.05
2	0.03
3	0.03
4	0.02
5	0.01
6	0.01
7	0.02
8	0.01
9	0.01
10	0.02
Average	0.021

Sample #	6
1	0.1
2	0.06
3	0.04
4	0.08
5	0.05
6	0.06
7	0.06
8	0.04
9	0.11
Average	0.067

Sample #	13-03-1 21.5-22
1	0.02
2	0.05
3	0.02
4	0.04

5	0.02
6	0.04
7	0.04
8	0.02
9	0.02
10	0.03
Average	0.03

Sample # 13-03-2

1	0.02
2	0.02
3	0.02
4	0
5	0.02
6	0
7	0.02
8	0
9	0.02
10	0.06
Average	0.018

Sample # 13-02-A-1 43

1	0.12
2	0.12
3	0.12
4	0.12
5	0.1
6	0.12
7	0.12
8	0.12
9	
10	
Average	0.1175

Sample # 13-02-2A 182-183

1	0.1
2	0.14
3	0.06
4	0.06
5	0.06
6	0.08

7	0.08
8	0.08
9	0.06
10	0.14
Average	0.086

Sample #	7
1	0.04
2	0.01
3	0.02
4	0.1
5	0.01
6	0.02
7	0.02
8	0.01
9	0.04
10	0.02
Average	0.029

Sample #	8
1	-0.21
2	-0.25
3	0.02
4	-0.11
5	-0.05
6	0.83
7	0.07
8	0.03
9	0.09
10	0
Average	0.042

Sample #	13-03-03 41-42
1	0.04
2	0.02
3	0.02
4	0.02
5	0.02
6	0.02
7	0.02
8	0.02

9	0.02
10	0.02
Average	0.022

/ ----------
/ CSV EXPORT [10/07/2014]
/ DATABASE [.\Gold Strike Rock Phys IP.gdb]
/ ----------
/
/X Y Z IP[0] IP[1] IP[2] IP[3] IP[4] IP[5]
//Flight 0
//Date 2014/10/06
Line 141

-37.5	141	-12.5	25.45	17.19	14.49	12.65	11.25	10.14
-37.5	141	-12.5	25.72	17.36	14.62	12.73	11.32	10.21
-37.5	141	-12.5	22.6	14.12	12.21	10.94	10.01	9.23
-37.5	141	-12.5	21.96	12.71	10.88	9.79	9	8.37
-37.5	141	-12.5	17.03	10.76	9.49	8.61	7.99	7.56
-62.5	141	-12.5	29.55	15.6	12.92	11.14	9.81	8.8
-62.5	141	-12.5	27.01	13.94	11.48	9.86	8.63	7.67
-62.5	141	-12.5	19.39	11.29	9.9	9.06	8.46	7.96
-62.5	141	-12.5	19.21	11.22	9.41	8.36	7.61	7.02
-62.5	141	-12.5	30.57	12.81	10.39	9.15	8.29	7.66
-87.5	141	-12.5	28.37	19.29	16.76	15.14	13.94	12.97
-87.5	141	-12.5	29.06	19.39	16.76	15.15	13.95	13
-87.5	141	-12.5	28.64	19.99	17.47	15.79	14.53	13.51
-87.5	141	-12.5	17.63	9.3	8.22	7.59	7.14	6.76
-87.5	141	-12.5	19	9.21	8.08	7.46	7.02	6.69
-87.5	141	-12.5	16.8	9.73	8.6	7.95	7.47	7.1
-112.5	141	-12.5	235.96	203.61	184.02	169.49	157.85	148.18
-137.5	141	-12.5	242.23	208.25	188.42	173.8	162.16	152.49
-137.5	141	-12.5	212.63	184.67	168.17	155.96	146.26	138.22
-162.5	141	-12.5	29.32	21.11	18.62	16.94	15.7	14.65
-162.5	141	-12.5	31.15	21.42	18.88	17.2	15.92	14.89
-162.5	141	-12.5	30.97	21.11	18.59	16.95	15.73	14.74
-162.5	141	-12.5	24.14	14.05	12.29	11.21	10.4	9.79
-162.5	141	-12.5	23.72	14.7	12.84	11.73	10.91	10.27
-162.5	141	-12.5	36.39	15.9	13.72	12.48	11.6	10.91
-187.5	141	-12.5	8.79	3.17	2.97	2.94	2.96	2.96
-187.5	141	-12.5	11.91	4.55	4.23	4.18	4.16	4.15
-187.5	141	-12.5	13.24	4.7	4.33	4.3	4.29	4.28
-212.5	141	-12.5	31.76	20.68	18.2	16.64	15.45	14.46
-212.5	141	-12.5	30.72	21.26	18.78	17.12	15.88	14.87
-212.5	141	-12.5	42.57	21.63	18.85	17.17	15.88	14.87
-212.5	141	-12.5	16.39	9.71	8.56	7.86	7.37	6.98
-212.5	141	-12.5	20	10.75	9.31	8.53	7.98	7.54
-212.5	141	-12.5	28.91	11.65	9.78	8.92	8.31	7.85
-237.5	141	-12.5	20.92	13.97	12.26	11.1	10.21	9.48
-237.5	141	-12.5	25.11	15.43	13.43	12.12	11.11	10.3

IP[6]	IP[7]	IP[8]	IP[9]	IP[10]	IP[11]	IP[12]	IP[13]	IP[14]
9.28	8.23	7.16	6.35	5.75	5.21	4.79	4.44	2.64
9.31	8.26	7.19	6.39	5.76	5.25	4.82	4.45	2.4
8.61	7.84	7.03	6.38	5.84	5.4	5.03	4.69	3.32
7.87	7.23	6.55	5.96	5.5	5.14	4.78	4.46	2.93
7.16	6.67	6.13	5.7	5.33	4.98	4.67	4.4	3.58
7.94	6.96	5.96	5.19	4.6	4.14	3.77	3.43	2.72
6.92	6	5.1	4.42	3.9	3.49	3.14	2.86	2.22
7.58	7.07	6.51	6.06	5.67	5.34	5.05	4.78	3.48
6.6	6.06	5.49	5.02	4.65	4.32	4.04	3.78	2.51
7.13	6.52	5.88	5.38	4.96	4.61	4.32	4.06	2.18
12.18	11.21	10.14	9.29	8.56	7.95	7.44	6.95	5.48
12.2	11.22	10.18	9.33	8.6	7.99	7.47	7	4.78
12.69	11.66	10.56	9.67	8.93	8.29	7.73	7.25	6.15
6.47	6.08	5.65	5.29	4.97	4.7	4.47	4.24	3.46
6.43	6.07	5.65	5.29	4.97	4.7	4.47	4.25	2.27
6.76	6.37	5.92	5.55	5.19	4.9	4.65	4.42	3.2
139.93	129.6	118.25	108.95	101.13	94.46	88.57	83.41	75.96
144.23	133.89	122.51	113.22	105.38	98.62	92.73	87.54	79.44
131.37	122.75	113.27	105.47	98.87	93.19	88.21	83.79	77.34
13.78	12.71	11.57	10.61	9.84	9.14	8.55	8.02	6.47
14.02	12.95	11.77	10.8	10	9.31	8.72	8.18	5.92
13.9	12.86	11.73	10.81	10.02	9.35	8.77	8.25	5.88
9.26	8.6	7.91	7.31	6.81	6.38	6.01	5.68	4.29
9.7	9.05	8.29	7.69	7.22	6.75	6.36	6	3.91
10.31	9.6	8.82	8.17	7.63	7.16	6.74	6.37	5.14
2.99	2.97	2.97	2.93	2.88	2.82	2.75	2.65	2.1
4.13	4.06	4.03	3.89	3.83	3.74	3.61	3.53	2.5
4.27	4.24	4.19	4.08	4	3.91	3.81	3.72	1.84
13.67	12.66	11.56	10.66	9.91	9.27	8.71	8.21	6.66
14.05	13.01	11.89	10.98	10.21	9.55	8.97	8.45	7.34
14.04	13.03	11.93	11.02	10.26	9.59	9.02	8.52	7.06
6.64	6.25	5.81	5.44	5.12	4.83	4.59	4.36	3.56
7.18	6.73	6.24	5.84	5.48	5.17	4.89	4.66	3.47
7.48	7	6.45	6.03	5.68	5.33	5.05	4.81	2.75
8.87	8.14	7.36	6.72	6.21	5.78	5.41	5.1	4.13
9.63	8.81	7.93	7.22	6.64	6.16	5.73	5.37	3.92

IP[15]	IP[16]	IP[17]	IP[18]	IP[19]	IP_Avg	N	T1X	R1X
1.21	2.11	2.19	2.15	2.04	5.2	1	-50	-25
0.69	1.89	2.06	2.04	1.96	5.1	1	-50	-25
3.11	3.28	3.03	2.78	2.56	5.4	1	-50	-25
3.11	3.3	3.04	2.81	2.59	5.1	1	-50	-25
3.68	3.45	3.14	2.86	2.63	4.9	1	-50	-25
2.75	2.76	2.64	2.52	2.4	5	1	-75	-50
2.34	2.38	2.29	2.2	2.1	4.4	1	-75	-50
3.98	4	3.63	3.3	3.05	5.3	1	-75	-50
3.01	3.09	2.75	2.51	2.27	4.5	1	-75	-50
3.21	3.57	3.13	2.79	2.52	5	1	-75	-50
5.58	5.39	4.84	4.39	4.02	8	1	-100	-75
5.79	5.69	5.07	4.56	4.16	8.1	1	-100	-75
5.88	5.5	4.98	4.56	4.18	8.4	1	-100	-75
3.5	3.42	3.14	2.9	2.68	4.7	1	-100	-75
3.69	3.83	3.41	3.08	2.82	4.7	1	-100	-75
3.6	3.67	3.35	3.05	2.8	4.8	1	-100	-75
69.05	63.21	57.94	53.43	49.53	92.5	1	-125	-100
73.1	67.29	61.86	57.14	53.12	96.6	1	-150	-125
71.54	66.36	61.68	57.64	54.12	91.2	1	-150	-125
6.71	6.31	5.71	5.21	4.79	9.2	1	-175	-150
6.99	6.76	6.01	5.44	4.97	9.4	1	-175	-150
7.14	6.91	6.14	5.54	5.07	9.4	1	-175	-150
4.76	4.66	4.21	3.84	3.53	6.4	1	-175	-150
5.29	5.3	4.7	4.25	3.88	6.8	1	-175	-150
5.35	5.23	4.74	4.33	3.99	7.5	1	-175	-150
2.39	2.46	2.31	2.15	2.02	2.7	1	-200	-175
3.14	3.32	3.05	2.82	2.64	3.6	1	-200	-175
3.61	3.83	3.45	3.17	2.92	3.8	1	-200	-175
6.83	6.57	5.94	5.41	4.95	9.3	1	-225	-200
7.01	6.58	6.03	5.55	5.15	9.5	1	-225	-200
7.11	6.82	6.2	5.68	5.25	9.9	1	-225	-200
3.73	3.58	3.29	3.04	2.81	4.8	1	-225	-200
4.03	3.99	3.59	3.31	3.06	5.2	1	-225	-200
4.2	4.39	3.91	3.55	3.26	5.6	1	-225	-200
4.92	4.49	4.04	3.67	3.38	6.1	1	-250	-225
4.06	4.06	3.73	3.45	3.21	6.3	1	-250	-225

R2X	Vp	I	Sp	QC	QC_RES	Type	ResMeas	Chg
0	8463.9	0.00003	-19.1	1	1	0 **		5.19
0	12683.4	0.000037	-8	1	1	0 **		5.1
0	3663.7	0.000031	-44.5	1	1	0 **		5.43
0	4554.9	0.000037	-45.5	1	1	0 **		5.13
0	8181.1	0.000062	-44	1	1	0 **		4.93
-25	12251.9	0.00001	32.5	1	1	0 **		5.04
-25	12440.6	0.00001	36.6	1	1	0 **		4.39
-25	14670.4	0.000022	37.1	1	1	0 **		5.34
-25	10275.2	0.000023	-2.1	1	1	0 **		4.46
-25	13334.7	0.000028	-6.8	1	1	0 **		5.05
-50	5031.6	0.000025	-15.4	1	1	0 **		8.01
-50	6050.5	0.00003	-12.5	1	1	0 **		8.07
-50	10087.1	0.00005	-11.5	1	1	0 **		8.35
-50	6041.6	0.00005	12.8	1	1	0 **		4.67
-50	3672.1	0.00003	6.9	1	1	0 **		4.69
-50	3301.9	0.000025	-5.3	1	1	0 **		4.82
-75	1835.4	0.000025	-34	1	1	0 **		92.54
-100	2295.6	0.000031	-44.8	1	1	0 **		96.6
-100	4377	0.00006	-26.9	1	1	0 **		91.18
-125	9229.7	0.000025	-38.1	1	1	0	0	9.15
-125	11293.9	0.00003	-34.9	1	1	0 **		9.36
-125	9986.1	0.000027	-28.3	1	1	0 **		9.38
-125	2473.4	0.000023	-24.3	1	1	0 **		6.44
-125	2997.2	0.000028	-18	1	1	0 **		6.8
-125	5785.8	0.000056	-12.8	1	1	0 **		7.45
-150	2125.3	0.000046	-11	1	1	0 **		2.68
-150	882.3	0.000024	-12.4	1	1	0 **		3.57
-150	1073.1	0.000028	-9.7	1	1	0 **		3.79
-175	3506	0.000023	13.6	1	1	0 **		9.29
-175	7029.8	0.000046	6.9	1	1	0 **		9.54
-175	8322.9	0.000056	2.7	1	1	0 **		9.87
-175	2695.6	0.000046	5.4	1	1	0 **		4.81
-175	3349.6	0.000056	7.7	1	1	0 **		5.22
-175	1699.8	0.000028	8.7	1	1	0 **		5.6
-200	10683.8	0.000022	-29.5	1	1	0 **		6.11
-200	13452	0.000026	-9.4	1	1	0 **		6.28

Q	Time	Stack	RsCheck	ColeTau	ColeM	ColeRMS	Name	Overload	
0.23	2000	15	251.3	0	0	0	not used	*	
0.24	2000	15	316.7	0	0	0	not used	*	
0.3	2000	15	117.8	0	0	0	not used	*	
0.34	2000	15	119.7	0	0	0	not used	*	
0.17	2000	15	125.7	0	0	0	not used	*	
2.42	2000	15	848.4	0	0	0	not used	*	
2.67	2000	15	626.6	0	0	0	not used	*	
0.2	2000	15	575.4	0	0	0	not used	*	
0.22	2000	15	425.8	0	0	0	not used	*	
0.58	2000	15	418.3	0	0	0	not used	*	
0.25	2000	15	197.1	0	0	0	not used	*	
0.25	2000	15	192.1	0	0	0	not used	*	
0.25	2000	15	198.8	0	0	0	not used	*	
0.2	2000	15	120.8	0	0	0	not used	*	
0.28	2000	15	116.8	0	0	0	not used	*	
0.23	2000	15	122.9	0	0	0	not used	*	
1.51	2000	15	54.7	0	0	0	not used	*	
1.92	2000	15	122.4	0	0	0	not used	*	
1.11	2000	15	63.8	0	0	0	not used	*	
0.23	2000	15	360.4	0	0	0	not used	*	
0.26	2000	15	358	0	0	0	not used	*	
0.27	2000	15	360.9	0	0	0	not used	*	
0.31	2000	15	567.5	0	0	0	not used	*	
0.22	2000	15	107	0	0	0	not used	*	
0.64	2000	15	104.6	0	0	0	not used	*	
0.17	2000	15	256.3	0	0	0	not used	*	
0.2	2000	15	54.9	0	0	0	not used	*	
0.25	2000	15	43.5	0	0	0	not used	*	
0.37	2000	15	148.8	0	0	0	not used	*	
0.27	2000	15	153.2	0	0	0	not used	*	
0.68	2000	15	146.9	0	0	0	not used	*	
0.19	2000	15	56.8	0	0	0	not used	*	
0.28	2000	15	58.3	0	0	0	not used	*	
0.56	2000	15	59.7	0	0	0	not used	*	
0.2	2000	15	460.9	0	0	0	not used		0
0.32	2000	15	519.1	0	0	0	not used		0

RxBat	TxBat	Temp	Date	DayTime	ResCalc	MF	Stn
*	*	*	10/2/2014	12:21:41	88633806	0	-37.5
*	*	*	10/2/2014	12:23:37	1.08E+08	0	-37.5
*	*	*	10/2/2014	12:26:56	37128714	0	-37.5
*	*	*	10/2/2014	12:29:00	38674764	0	-37.5
*	*	*	10/2/2014	12:31:01	41454127	0	-37.5
*	*	*	10/3/2014	12:55:14	3.85E+08	0	-62.5
*	*	*	10/3/2014	12:59:32	3.91E+08	0	-62.5
*	*	*	10/3/2014	13:36:34	2.09E+08	0	-62.5
*	*	*	10/3/2014	13:42:21	1.4E+08	0	-62.5
*	*	*	10/3/2014	13:44:33	1.5E+08	0	-62.5
*	*	*	10/3/2014	13:48:30	63229170	0	-87.5
*	*	*	10/3/2014	13:50:41	63360980	0	-87.5
*	*	*	10/3/2014	13:52:41	63378800	0	-87.5
*	*	*	10/3/2014	13:56:41	37960425	0	-87.5
*	*	*	10/3/2014	13:58:52	38454129	0	-87.5
*	*	*	10/3/2014	14:00:53	41493077	0	-87.5
*	*	*	10/3/2014	14:04:33	23063706	0	-112.5
*	*	*	10/3/2014	14:06:33	23264431	0	-137.5
*	*	*	10/3/2014	14:08:33	22841539	0	-137.5
*	*	*	10/6/2014	10:27:43	1.16E+08	0	-162.5
*	*	*	10/6/2014	10:29:53	1.18E+08	0	-162.5
*	*	*	10/6/2014	10:32:50	1.16E+08	0	-162.5
*	*	*	10/6/2014	10:37:11	33784814	0	-162.5
*	*	*	10/6/2014	10:39:18	33628971	0	-162.5
*	*	*	10/6/2014	10:41:31	32458415	0	-162.5
*	*	*	10/6/2014	10:45:30	14515136	0	-187.5
*	*	*	10/6/2014	10:47:35	11549309	0	-187.5
*	*	*	10/6/2014	10:49:44	12040219	0	-187.5
*	*	*	10/6/2014	10:53:24	47888114	0	-212.5
*	*	*	10/6/2014	10:56:28	48010516	0	-212.5
*	*	*	10/6/2014	10:59:27	46691224	0	-212.5
*	*	*	10/6/2014	11:03:09	18409542	0	-212.5
*	*	*	10/6/2014	11:05:01	18791418	0	-212.5
*	*	*	10/6/2014	11:07:05	19071415	0	-212.5
11.2	0	16.2	10/7/2014	10:02:23	1.53E+08	0	-237.5
11.2	0	17.2	10/7/2014	10:04:50	1.63E+08	0	-237.5

Topo	sample	length	volume	calcappres	VP_SIU	Length_SIU	aREA_sIU	Area
*	13-03-3	8	16.08	708.85	8.46	0.08	0.000201	2.01
*	13-03-3	8	16.08	861.27	12.68	0.08	0.000201	2.01
*	13-03-2	7.3	29.35	650.82	3.66	0.07	0.000402	4.02
*	13-03-2	7.3	29.35	677.92	4.55	0.07	0.000402	4.02
*	13-03-2	7.3	29.35	726.64	8.18	0.07	0.000402	4.02
*	13-02-A1 4	5.4	43.42	18241.74	12.25	0.05	0.000804	8.04
*	13-02-A1 4	5.4	43.42	18522.68	12.44	0.05	0.000804	8.04
*	13-02-A1 4	5.4	43.42	9928.43	14.67	0.05	0.000804	8.04
*	6	6	76	9431.31	10.28	0.06	0.001267	12.66667
*	6	6	76	10053.94	13.33	0.06	0.001267	12.66667
*	8	7.24	195	7487.3	5.03	0.07	0.002693	26.9337
*	8	7.24	195	7502.91	6.05	0.07	0.002693	26.9337
*	8	7.24	195	7505.02	10.09	0.07	0.002693	26.9337
*	13-03-1 21	5.4	21.71	899.53	6.04	0.05	0.000402	4.02
*	13-03-1 21	5.4	21.71	911.22	3.67	0.05	0.000402	4.02
*	13-03-1 21	5.4	21.71	983.24	3.3	0.05	0.000402	4.02
*	7	6.38	59	1064.12	1.84	0.06	0.000925	9.247649
*	7	6.38	59	1073.38	2.3	0.06	0.000925	9.247649
*	7	6.38	59	1053.87	4.38	0.06	0.000925	9.247649
*	5	6.44	141	12551.47	9.23	0.06	0.002189	21.89441
*	5	6.44	141	12798.85	11.29	0.06	0.002189	21.89441
*	5	6.44	141	12574.14	9.99	0.06	0.002189	21.89441
*	1	5.42	102	3733.99	2.47	0.05	0.001882	18.81919
*	1	5.42	102	3716.77	3	0.05	0.001882	18.81919
*	1	5.42	102	3587.39	5.79	0.05	0.001882	18.81919
*	3	6.84	146	1441.82	2.13	0.07	0.002135	21.34503
*	3	6.84	146	1147.22	0.88	0.07	0.002135	21.34503
*	3	6.84	146	1195.98	1.07	0.07	0.002135	21.34503
*	2	6.4	141	5247.31	3.51	0.06	0.002203	22.03125
*	2	6.4	141	5260.73	7.03	0.06	0.002203	22.03125
*	2	6.4	141	5116.17	8.32	0.06	0.002203	22.03125
*	4	4.96	138	3287.07	2.7	0.05	0.002782	27.82258
*	4	4.96	138	3355.25	3.35	0.05	0.002782	27.82258
*	4	4.96	138	3405.25	1.7	0.05	0.002782	27.82258
*	13-02A 18	5.4	43.42	7230.44	10.68	0.05	0.000804	8.04
*	13-02A 18	5.4	43.42	7703.29	13.45	0.05	0.000804	8.04

sample	Vp	I	Sp	length	volume	Area		IP_Avg	
13-03-3	8463.9	0.00003	-19.1	8	16.08	2.01		5.2	
13-03-3	12683.4	0.000037	-8	8	16.08	2.01		5.1	
13-03-2	3663.7	0.000031	-44.5	7.3	29.35	4.02		5.4	
13-03-2	4554.9	0.000037	-45.5	7.3	29.35	4.02		5.1	
13-03-2	8181.1	0.000062	-44	7.3	29.35	4.02		4.9	
13-02-A1 4	12251.9	0.00001	32.5	5.4	43.42	8.04		5	
13-02-A1 4	12440.6	0.00001	36.6	5.4	43.42	8.04		4.4	
6	10275.2	0.000023	-2.1	6	76	12.66667		4.5	
6	13334.7	0.000028	-6.8	6	76	12.66667		5	
8	5031.6	0.000025	-15.4	7.24	195	26.9337		8	
8	6050.5	0.00003	-12.5	7.24	195	26.9337		8.1	
8	10087.1	0.00005	-11.5	7.24	195	26.9337		8.4	
13-03-1 21	6041.6	0.00005	12.8	5.4	21.71	4.02		4.7	
13-03-1 21	3672.1	0.00003	6.9	5.4	21.71	4.02		4.7	
13-03-1 21	3301.9	0.000025	-5.3	5.4	21.71	4.02		4.8	
7	1835.4	0.000025	-34	6.38	59	9.247649		92.5	
7	2295.6	0.000031	-44.8	6.38	59	9.247649		96.6	
7	4377	0.00006	-26.9	6.38	59	9.247649		91.2	
5	9229.7	0.000025	-38.1	6.44	141	21.89441		9.2	
5	11293.9	0.00003	-34.9	6.44	141	21.89441		9.4	
5	9986.1	0.000027	-28.3	6.44	141	21.89441		9.4	
1	2473.4	0.000023	-24.3	5.42	102	18.81919		6.4	
1	2997.2	0.000028	-18	5.42	102	18.81919		6.8	
1	5785.8	0.000056	-12.8	5.42	102	18.81919		7.5	
3	2125.3	0.000046	-11	6.84	146	21.34503		2.7	
3	882.3	0.000024	-12.4	6.84	146	21.34503		3.6	
3	1073.1	0.000028	-9.7	6.84	146	21.34503		3.8	
2	3506	0.000023	13.6	6.4	141	22.03125		9.3	
2	7029.8	0.000046	6.9	6.4	141	22.03125		9.5	
2	8322.9	0.000056	2.7	6.4	141	22.03125		9.9	
4	2695.6	0.000046	5.4	4.96	138	27.82258		4.8	
4	3349.6	0.000056	7.7	4.96	138	27.82258		5.2	
4	1699.8	0.000028	8.7	4.96	138	27.82258		5.6	
13-02A 18	10683.8	0.000022	-29.5	5.4	43.42	8.04		6.1	
13-02A 18	13452	0.000026	-9.4	5.4	43.42	8.04		6.3	

calcappres	Average IP	Average Res
708.85		
861.27	5.15	785.06
	0.070711	107.7772
650.82		
677.92		
726.64	5.133333	685.1267
	0.251661	38.42031
18241.74		
18522.68	4.7	18382.21
	0.424264	198.6546
9431.31		
10053.94	4.75	9742.625
	0.353553	440.2659
7487.3		
7502.91		
7505.02	8.166667	7498.41
	0.208167	9.67921
899.53		
911.22		
983.24	4.733333	931.33
	0.057735	45.33376
1064.12		
1073.38		
1053.87	93.43333	1063.79
	2.818392	9.759185
12551.47		
12798.85		
12574.14	9.333333	12641.49
	0.11547	136.7512
3733.99		
3716.77		
3587.39	6.9	3679.383
	0.556776	80.13247
1441.82		
1147.22		
1195.98	3.366667	1261.673
	0.585947	157.905
5247.31		
5260.73		
5116.17	9.566667	5208.07
	0.305505	79.87009
3287.07		
3355.25		
3405.25	5.2	3349.19
	0.4	59.3226
7230.44		
7703.29	6.2	7466.865
	0.141421	334.3554

MOLSPIN 2

Note **** There are no dirrections to these samples so only the intensity is valid

Calibration	1	2	3	4	5	6
						Error
Time						± 3min
Intensity						±1.0000
Dec						±5 Degrees

Sample #	6	Earth Field	57000	
Plane Azimuth		Volume of cube	97.34	
Plane Dip		Mag susc	6.66667E-05	SI units
Intensity	0.4243	Remanent Mag	2.332751313	mA/m
Inclination	37.3	Remanent Mag	0.002332751	A/m SI units
Declination	129.7	Remanent mag fi	2.931421755	nT
Avrg_Int	0.4243	Remanent mag d	129.7	
		Remanent mag ir	37.3	
	Sample volume	Koenigsberger ra	0.771426778	
Volume	17.705			

Sample #	8	Earth Field	57000	
Plane Azimuth		Volume of cube	97.34	
Plane Dip		Mag susc	0.000042	SI units
Intensity	0.0687	Remanent Mag	0.390816317	mA/m
Inclination	2.6	Remanent Mag	0.000390816	A/m SI units
Declination	105.8	Remanent mag fi	0.491114268	nT
Avrg_Int	0.0687	Remanent mag d	105.8	
		Remanent mag ir	2.6	
	Sample volume	Koenigsberger ra	0.205143805	
Volume	17.111			

Sample #	13-02-2A 182-183	Earth Field	57000	
Plane Azimuth		Volume of cube	97.34	
Plane Dip		Mag susc	0.000086	SI units
Intensity	1.5694	Remanent Mag	4.268501383	mA/m
Inclination	-81.4	Remanent Mag	0.004268501	A/m SI units
Declination	152	Remanent mag fi	5.363957035	nT
Avrg_Int	1.5694	Remanent mag d	152	
		Remanent mag ir	-81.4	
	Sample volume	Koenigsberger ra	1.094238481	
Volume	35.789			

Sample #	13-01-2A 43	Earth Field	57000	
Plane Azimuth		Volume of cube	97.34	

Plane Dip		Mag susc	0.0001175	SI units	
Intensity	0.0443	Remanent Mag	0.32613538	mA/m	
Inclination	-56.8	Remanent Mag	0.000326135	A/m	SI units
Declination	275.1	Remanent mag fi	0.409833806	nT	
Avrg_Int	0.0443	Remanent mag d	275.1		
		Remanent mag ir	-56.8		
	Sample volume	Koenigsberger ra	0.061192058		
Volume	13.222				

AURORA GEOSCIENCES

NORTHERN GEOLOGICAL & GEOPHYSICAL CONSULTANTS

YELLOWKNIFE - WHITEHORSE - JUNEAU

34A Laberge rd. Whitehorse, YT, Y1A 5Y9 (p) 867.668.7672

MEMORANDUM

To: Trevor Bremner
Bill Chornobay

Date: August XX, 2014

From: Louis Rosenthal
Dave Hildes

Re: 2014 South Plateau 3D DCIP Field Report

This memorandum describes 3D DC/IP surveyscompleted for GoldstrikeResources Ltd.on the soul plateau property between July29th and August 6th, 2014. The purpose of the survey was to measure the resistivity and chargeability across gold showings on the property.

Four AGL personnel left Whitehorse in a pickup loaded with the camp and geophysical equipment on the morning of August 6th. They metDaithi of Druid Exploration at the Black Sheep Aviation float base in Mayo, Yukon, and loaded the equipment into a DeHavilland Beaver and Otter. The planes landed and unloaded the equipment at Spit Lake, and were met by a Jet ranger from Trans North Helicopters, which ferried equipment and personnel to the South Plateau property. The crew set up a 2 tent camp that evening and the next morning, and started the survey on the afternoon of July 30th, 2014.

The source of signal for the survey was a GDD TxII3.6 kW steady-voltage IP transmitter which creates potentials up to 2400V and 3600 watts of power. The transmitter array consisted of a stationary electrode south of the survey area (581264.05E 7017393.16N for detail grids and 581313.75E and 7017095.93N for coarse grids) and roving current injection site. The transmitter was powered by a 5 kW Honda Gasoline generator. Total fuel consumption was approximately 60 L. The primary voltage and chargeability was measured and recorded by two Iris Elrec-Pro 10-channel receivers plugged into stainless steel electrode arrays.

The survey design consisted of detail 5m dipole swaths and coarse 15 & 25 m dipoles swaths (see location map include with this report). The four detailed swaths are oriented roughly E-W and consist of a 20*5m dipole receiver array that is flanked by current lines spaced 15 or 20m perpendicular to the receiver array with current injection stations every 5m. These swaths also used current injections points in line with the receiver, spaced 60, 70, 80, 90 100 and 130 m from the center point. Data surveyed on the extensions used 10*10m dipoles to increase signal and depth sensitivity. In the final figures and datasets, the lines are named by averaging the name of the current and receiver line. Note that on a given swath the extensions will be the same for both lines of data.

The three coarse swaths are oriented N-S and consist of 4*25m 12*15m 4*25m dipole receiver array flanked by current lines spaced 50 m on either side of the receiver array. The extensions for the coarse swaths had current injections points 50, 100, 150, 200, 250, 350 450 and 550 from either end of the line. Line names in the figures and databases the average of the current and receiver line name.

These arrays produce two distinct datasets/pseudosections for each line of data, defined by the relationship of the current electrode to the receiver dipole. Data is group according to which side of the receiver dipole the transmitter dipole is located. On the flanking current lines, there are many readings where the transmitter electrode is at the same station as one of the receiver electrodes. These readings are subject to null coupling and

are rejected from the database. Stacked sections of the apparent chargeability, calculated resistivity and chargeability error are included with this report.

Data quality was excellent for the vast majority of the survey. Due to the rocky felsenmeer nature of the ground, the current injections were relatively small, however the high resistivity of the rock made for very clean readings.

a. Crew

The following personnel conducted the survey:

Louis Rosenthal	Crew Chief	August 9-19th,2014
Mac Clohan	Geophysical Technician	August 9-19th, 2014
Matthew Ford	Geophysical Technician	August 9-16th, 2014
Shawn Scott	Geophysical Technician	August 9-16th, 2014

b. Equipment

The crew was equipped with the following instruments and equipment:

IP receiver	2 - Iris Elrec Pro 10 channel IP receiver s/n: 165, 122
IP transmitter	2 - GDD TxII 3.6 kW s/n:266, 246
Generator	1 - Honda Ex5000 5kW generator
IP Equipment	1 - Repair tools and spare IP parts
	40 - Stainless steel electrodes
	6 km - 18 gauge wire
	2 - Georeels
	3 - Spools
Other	1 - laptop with Geosoft IP package
	5 - Garmin handheld non-differential GPS
	5 - Icom handheld radios
	1 - Icom Base Radio

b.Survey Location

The South Plateau Property is located approximately 80 km north of Whitehorse and is accessed by fixed wing aircraft and helicopter

c. Survey Specifications

GPS

Geographic datum & projection:	NAD83 Zone 3 UTM coordinates
Grid location:	The grid locations were provided by Trevor Bremner.
Station marking:	Stations were situated using handheld Garmin GPS's for the coarse grids. The center and strike of the detail grids was located using a

	handheld GPS, individual stations were determined by using a chain and prism.
Grid Registration	GPS location for each station of the coarse grids is determined by examining the track logsof the operators.The GPS locations for the detail grids was determined by interpolating between the GPS points taken at the end of each transmitter and receiver lines.
3D DCIP	
Array:	Modified Pole-dipole
Dipole Spacing:	5, 15 and 25 m
Dipoles range:	N=1-65
Transmitter settings:	Time domain, 50% duty cycle, reversing polarity, 0.125 Hz.
Receiver Settings:	Semi-logarithmically spaced time gates
Stacks:	15 stacks per reading
Repeats	If the initial reading had an S.D greater than 5 mV/V or if the reading was suspected for any reason, the reading was repeated until the operator determined the data was acceptable or unattainable.
Distant Electrode:	The distant electrode wassouth of the survey area, in a marsh at the base of the mountain for the detail grid. It was located in a wet area 500 m further up the hill for the coarse grids.

d. Data Processing

Data was downloaded from the receivers nightly and imported into Geosoft Oasis Montaj IP extension.GPS databases are created from the track log and waypoints in the GPS dump files. All electrodes are geo-referenced using a cross channel database lookup. Every reading is inspected and readings which do not repeat or are suspect for any reason are rejected using the Oasis Montaj's IP quality control tool.

The apparent resistivity is recalculated using a four electrode equation assuming a homogeneous earth using the geo-referenced coordinates. The apparent resistivity and total chargeability are averaged using a weighted mean based on the number of stacks and the standard deviation of the chargeability.

Positive polarity was assigned to the primary voltage so that when the receiver dipole is north or east of the roving transmitter location and negative polarity when it is south or west of the roving dipole. Mask channels are created to organize the final data into groups defined by the relationship between the transmitter and receiver dipoles.

Stacked sections are calculated for each group of data at for both the coarse and details surveys using the geosoft executable. These staked sections have common colour scales. The gridding algorithm in the geosoft executable is not optimized for variable dipole spacing, so there are many artifacts in the final grids. This has been reported to geosoft and will be fixed in a future release. New stacked sections will be provided after the gridding problem has been addressed.

Table 1 lists the name and description of the channels in the final databases.

Table 1: List and description of the channels in the final databases

Channel Name	Description
X	Georeferenced Plot point -Easting

Y	Georeferenced Plot point -Northing
Z	Georeferenced Plot point - Elevation
__X	Local Coordinate Plot point - Station
__Y	Local Coordinate Plot point - Line
__Z	Local Coordinate Plot point - Depth
Stn	Stn, defined by geosoft as the midpoint between RX1 and TX1
stn_utme	Easting of Stn
stn_utmn	Northing of Stn
Topo	Elevation of Stn
T1X	Local Coordinate of T1X (roving current electrode)
T1X_	UTM Easting Nad 83 Zone 3 coordinate of T1X
T1Y_	UTM Northing Nad 83 Zone 3 coordinate of T1X
T1Z_	Elevation of T1X
t2_Z	Elevation of T2X
T2X	Dummy value local coordinate of infinite electrode
T2X_	UTM Easting Nad 83 Zone 3 coordinate of T2X
T2y_	UTM Northing Nad 83 Zone 3 coordinate of T2X
R1X	Local Coordinate of potential electrode 1
R1X_	UTM Easting Nad 83 Zone 3 coordinate of R1X
R1Y_	UTM Northing Nad 83 Zone 3 coordinate of R1X
R1Z_	Elevation of R1X
R2X	Local Coordinate of potential electrode 2
R2X_	UTM Easting Nad 83 Zone 3 coordinate of R2X
R2Y_	UTM Northing Nad 83 Zone 3 coordinate of R2X
R2Z_	Elevation of R2X
Date	Date of data acquisition
DayTime	Time of data acquisition
Type	Geosoft indicator of array type
Time	Length of the reading window
Stack	Number of transmitter cycles measured during the course of the reading
RsCheck	Contact resistance of potential electrodes (kOhm)
IP_Index	Necesarry channel for Geosoft Database
IP_Mask[0]	Geosoft mask value in the 40-80 msofftime window (mV/V)
IP_Mask[1]	Geosoft mask value in the 80-120 msofftime window (mV/V)
IP_Mask[2]	Geosoft mask value in the 120-160 msofftime window (mV/V)
IP_Mask[3]	Geosoft mask value in the 160-200 msofftime window (mV/V)
IP_Mask[4]	Geosoft mask value in the 200-240 msofftime window (mV/V)
IP_Mask[5]	Geosoft mask value in the 240-280 msofftime window (mV/V)
IP_Mask[6]	Geosoft mask value in the 280-360 msofftime window (mV/V)
IP_Mask[7]	Geosoft mask value in the 360-440 msofftime window (mV/V)
IP_Mask[8]	Geosoft mask value in the 440-520 msofftime window (mV/V)
IP_Mask[9]	Geosoft mask value in the 520-600 msofftime window (mV/V)
IP_Mask[10]	Geosoft mask value in the 600-680 msofftime window (mV/V)

IP_Mask[11]	Geosoft mask value in the 680-760 msofftime window (mV/V)
IP_Mask[12]	Geosoft mask value in the 760-840 msofftime window (mV/V)
IP_Mask[13]	Geosoft mask value in the 840-1000 msofftime window (mV/V)
IP_Mask[14]	Geosoft mask value in the 1000-1160 msofftime window (mV/V)
IP_Mask[15]	Geosoft mask value in the 1160-1320 msofftime window (mV/V)
IP_Mask[16]	Geosoft mask value in the 1320-1480 msofftime window (mV/V)
IP_Mask[17]	Geosoft mask value in the 1480-1640 msofftime window (mV/V)
IP_Mask[18]	Geosoft mask value in the 1640-1800 msofftime window (mV/V)
IP_Mask[19]	Geosoft mask value in the 1800-1960 msofftime window (mV/V)
Sp	Spontaneous potential (mV/V)
ResCalc	Apparent resistivity calculated by Geosoft (without correction for proximal infinite) (Ohm*m)
ResMeas	Apparent resistivity calculated by the receiver (local coordinate) (Ohm*m)
Vp	Primary voltage measured 1260 into the ontime window (mV)
VP_Final	Primary voltage normalized by the current then averaged between repeated readings weighted according to their standard deviation. (mV/mA)
QC_RES	Quality control for the resistivity channel
Recalc_res	Resistivity calculated using four electrode equation.
Res_Final	Final Calculated Resistivity averaged between repeated readings weighted according to their standard deviation. (ohm.m)
I	Transmitter current (A)
Chg	Average chargeability calculated by the receiver
IP[0]	Normalized Voltage measurement in the 40-80 msofftime window (mV/V)
IP[1]	Normalized Voltage measurement in the 80-120 msofftime window (mV/V)
IP[2]	Normalized Voltage measurement in the 120-160 msofftime window (mV/V)
IP[3]	Normalized Voltage measurement in the 160-200 msofftime window (mV/V)
IP[4]	Normalized Voltage measurement in the 200-240 msofftime window (mV/V)
IP[5]	Normalized Voltage measurement in the 240-280 msofftime window (mV/V)
IP[6]	Normalized Voltage measurement in the 280-360 msofftime window (mV/V)
IP[7]	Normalized Voltage measurement in the 360-440 msofftime window (mV/V)
IP[8]	Normalized Voltage measurement in the 440-520 msofftime window (mV/V)
IP[9]	Normalized Voltage measurement in the 520-600 msofftime window (mV/V)
IP[10]	Normalized Voltage measurement in the 600-680 msofftime window (mV/V)
IP[11]	Normalized Voltage measurement in the 680-760 msofftime window (mV/V)
IP[12]	Normalized Voltage measurement in the 760-840 msofftime window (mV/V)
IP[13]	Normalized Voltage measurement in the 840-1000 msofftime window (mV/V)
IP[14]	Normalized Voltage measurement in the 1000-1160 msofftime window (mV/V)
IP[15]	Normalized Voltage measurement in the 1160-1320 msofftime window (mV/V)
IP[16]	Normalized Voltage measurement in the 1320-1480 msofftime window (mV/V)
IP[17]	Normalized Voltage measurement in the 1480-1640 msofftime window (mV/V)
IP[18]	Normalized Voltage measurement in the 1640-1800 msofftime window (mV/V)
IP[19]	Normalized Voltage measurement in the 1800-1960 msofftime window (mV/V)
IP_Avg	Average Chargeability calculated by the receiver
IP_Avg_Final	Final Apparent chargeability averaged between repeated readings weighted according to

	their standard deviation. (mV/V)
IP_err_FInal	Final Chargeability error averaged between repeated readings weighted according to their standard deviation. (mV/V)
MF	Calculated Metal Factor
N	The dipole number in the array
Q	Standard deviation of the average chargeability during the reading (mV/V)
QC	Quality control for IP_Avg Channel
Mask_e (or N)	Mask channel used to group data
Mask_w (or S)	Mask channel used to group data
IP_Avg_e(or N)	IP_Avg_final * Mask E (or N)
IP_Avg_w(or S)	IP_Avg_final * Mask W (or S)
Res_E(or N)	Res_Final * mask_e (or N)
Res_w(or S)	Res_Final * mask_w (or S)
IP_err_E(or N)	IP_err_Final * mask E (or N)
IP_err_W(or S)	IP_err_Final *mask W (or S)

e. Products

The following files are included in the digital version of this report:

File / Folder name	Description of contents
\Daily Log\	Daily log, Production summary and Personnel Tracking Sheet in PDF format
\Databases\	Final Databases in GDB and ASCII format
\Figures\	Stacked Sections,grid location maps in PDF format
\Raw\	Raw IP receiver,and GPS receiver dump files organized by date

Respectfully submitted,

Louis Rosenthal, B Sc.